NICKEL-CADMIUM CELLS

Edward J. Rubin
Michael J. Turchan

Tyco Laboratories, Inc.
16 Hickory Drive
Waltham, Massachusetts 02154

Final Report for Period 30 March 1972 - 30 May 1973

August 1974

1. Report No.	2. Government Accession No.	3. Recipient's Catalog No.
4. Title and Subtitle		5. Report Date
		August 1974
NICKEL-CADMIUM CELLS		6. Performing Organization Code
7. Author(s)		8. Performing Organization Report No.
Edward J. Rubin, Michael J. Turchan		C227
		10. Work Unit No.
9. Performing Organization Name and Address		
Tyco Laboratories, Inc.		
16 Hickory Drive		11. Contract or Grant No.
Waltham, Massachusetts 02154		NAS5-23102
		13. Type of Report and Period Covered
12. Sponsoring Agency Name and Address		Final Report 4/30/72 - 5/30/73
NASA Goddard Space Flight Center		
Greenbelt Road.		14. Sponsoring Agency Code
Greenbelt, Maryland 20771		

15. Supplementary Notes

16. Abstract

The objective of this contract was to design a high energy density nickel cadmium cell of aerospace quality. The approach used was to utilize manufacturing techniques which produce highly uniform and controlled starting materials in addition to improvements in the overall design. Parameters controlling the production of plaque and both positive and negative plate were studied. Quantities of these materials were produced and prototype cells were assembled to test the proposed design.

17. Key Words (Suggested by Author(s))	18. Distribution Statement		
Nickel-Cadmium Cell Nickel Plaque Battery Plate Cell Design			
19. Security Classif. (of this report)	20. Security Classif. (of this page)	21. No. of Pages	22. Price*
Unclassified	Unclassified	111	

ABSTRACT

The objective of this contract was to design a high energy density nickel cadmium cell of aerospace quality. The specific energy density goal was to approach 20 Whr/lb. Improvement of the energy density of existing cells was undertaken by first analyzing the factors having the greatest effect upon it. First, the weight contributions of the individual components of a typical commercial cell were quantified. Next, improvements, i.e., decreases in component weights were shown to be possible in a number of areas. Specifically, plaque substrate weights could be reduced by selecting smaller wire diameter screen without affecting the plaque strength. In addition, major weight savings could be achieved by reducing the sinter Ni plaque weight yet not detrimentally affecting plate conductivity, mechanical strength, or pore structure. Such improvements suggest the utilization of manufacturing techniques which produce highly uniform and controlled starting materials in addition to improvements in the overall cell design. In addition to the component weight reduction, increased utilization of the active materials within the pores of the improved sintered Ni plaque was expected in conjunction with the appropriate electrolyte level and plate loading levels.

Sintered Ni plaque was developed on light-weight woven nickel screen substrate which exhibited improved porosity (up to $> 84\%$ powder porosity). The plaque had, in addition, a pore volume distribution which has been shown in previous studies to be favorable to good utilization of the subsequently deposited active materials. This improved plaque material was subsequently used to establish the optimum parameters for the impregnation of the active materials. The efficient, high temperature electrochemical impregnation method was used to produce uniform, highly predictable positive and negative plate at the experimental, batch process level. Parameters determined here were then applied to the manufacture of plaque and plate material for

the assembly of test cells. Although difficulties in the "scale up" from experimental batch quantities to mass quantities of plaque material hindered the theoretical improvements expected to be manifested in the final product, cells were assembled and tested with resultant energy densities of 15 Whr/lb.

Table of Contents

List of Illustrations

List of Illustrations (continued)

List of Tables

List of Tables (continued)

L· INTRODUCTION

The objective of this program was to design, develop, and produce well-controlled and uniform materials for aerospace quality nickel cadmium cells and batteries. Specific design goals were to control plaque gauge to ± 0.0005 in. and plaque weight to ± 0.05 g/in.^{2} Goals for plate capacity variability were ± 2% at the one σ level for the positive plate and ± 3% for the negative plate. An additional program goal was to develop design criteria for the manufacture of cells with an energy density approaching 20 Whr/lb. The cycling demands and operational temperatures of synchronous and near earth orbits have been considered.

To accomplish these goals, a four phase program was carried out to study and optimize in a logical manner: (1) the cell design, (2) plaque development and manufacture, (3) plate development and manufacture, and (4) fabrication of hardware to evaluate plate and operating cell characteristics versus the design goals. The first phase was carried out by analyzing cell components which are the major weight constituents. On this basis improvement of the cells' energy density was realized by decreasing various component weights. During the second phase of the program, NI sinter plaque embodying the necessary high degree of quality and uniformity was produced which substantiated our projected weight savings in the proposed cell design. In the third portion of the contract, the development of optimized conditions and procedures for the manufacture of both positive and negative plate utilizing the high temperature electrochemical method of impregnation was carried out and further substantiated·the validity of the proposed cell design. Finally, hardware in the form of 4 Ahr cells was fabricated on an experimental basis. Later, 12 Ahr cells, manufactured to the final design criteria were tested.

It was determined theoretically, that in a 20 Ahr size cell a modest increase in energy density could be realized. In the 12 Ahr configuration the ratio of active cell components to case weight severely hampers improvement of energy density.

1

II. CELL DESIGN

A. Design Considerations for Higher Energy Density Cells

Factors influencing the energy density of sintered plate nickel-cadmium cells can be categorized as follows:

1. Weight of the hardware (i.e., cell case, terminals electrolyte, tabs, etc.),

2. Weight of the supporting substrate (mesh, perforated sheet, expanded metal, etc.),

3. Weight of the sinter structure,

4. Weight and efficiency (utilization) of the active materials, initially and as a function of time,

5. Polarization characteristics of the cell.

Some improvements in the weight (hence, energy density) of commonly used hardware are possible through the use of lighter weight case materials (e.g., Ti, plastic, etc.) These improvements are considered beyond the scope of the effort. However, the weight of the supporting substrate can be reduced measurably. For example, by reducing the wire size from 0.007 in. to 0.006 in. for a woven Ni mesh, the substrate weight is decreased by 25%.

Also important is the weight of the sintered structure, since the Ni sinter can contribute as much as 35%[1] of the plate weight. Reducing the weight of the sinter without detrimentally affecting plate conductivity, mechanical strength, and plate pore structure would increase the energy density of the cell. Of equal if not greater significance is the weight of the active material contained in the porous plates. With a controversial exception for the positive plate, the active materials have fixed

electrochemical equivalents (i.e., coulombs per mole or unit weight). The utilization of these active materials can vary[1] with the pore structures of the plaque, the quantity of electrolyte available and the loading level. Therefore, increasing the utilization of active material in the plates by optimizing plaque structure adds to the energy density of a cell.

B. Conventional Cell Analysis

In order to determine the proper approach to improved cell design, data on existing cells was developed and analyzed. The initial step taken involved analyzing the weight of a conventional 20 Ahr rated aerospace cell equipped with a third electrode. These data, presented in Table I, indicate which cell components are major weight constituents. It is the reduction in weight of those heavy components (i.e., positive plate, negative plate, cell case) that has the largest impact on cell weight.

Table I. Component Weight of a 20-Ahr Cell

Total cell weight		917.0 g
Nine negative electrodes	243.22 g	
Ten positive electrodes	292.41 g	
Stainless steel case (0.031 in. thick)	214.91 g	
Cell top, nylon screen, 3rd electrode	64.36 g	
Separator	10.63 g	
Subtotal Weight	825.53 g	
Electrolyte weight by difference		91.47 g

These data indicate that the case accounts for 23.5% of the cell weight. Therefore, a reduction of 20% of the case thickness (i.e., reduced from 0.031 to 0.025 in.) will decrease the weight of the cell by 4.7 g. The other major weight components are the negative and positive electrodes comprising 26.5% and 31.8% of the total cell weight, respectively. It is apparent from these data that a reduction in plate weight is significant and would have a measurable effect on increasing cell energy density.

4

C. Improved Cell Design

The plate weight can be broken down into three constituents; namely, the substrate, the plaque, and the active material. These components were analyzed to determine their contribution to the plate weight. Data are presented in Tables II, III, and IV. Using these data the following cell design was postulated.

As an example of these calculations, a cell rated to deliver 20 Ahr is chosen. It should be noted that plate weights can be proportionately increased or reduced depending on cell size and capacity, this can have profound effects on the final energy density.

1. 20-Ahr cell

a. Cell rated capacity is 20 Ahr (assumption).

b. To assure cell delivers the rated capacity, set tolerance such that the cell will deliver 22 Ahr (safety factor).

c. The positive plate nominally delivers 80% efficiency in the starved state; therefore:

$$\frac{22 \text{ Ahr}}{0.8 \text{ efficiency}} = \begin{array}{l} 27.5 \text{ Ahr of positive active material} \\ \text{in the flooded state} \end{array}$$

d. At the designed loading density of 7 Ahr per $in.^3$,

$$\frac{27.5 \text{ Ahr}}{7 \text{ Ahr/in.}^3} = 3.93 \text{ in.}^3 \text{ of plate are required.}$$

e. Using as a boundary condition the accepted size package for a 20-Ahr rated cell, trial and error calculations were made to determine plate thickness. Thus, at a positive plate thickness of 0.028 in.

$$\frac{3.93 \text{ in.}^3}{0.028 \text{ in.}} = 140 \text{ in.}^2 \text{ of plate area}$$

f. Using these same boundary conditions, a 14-$in.^2$ plate is used, thus providing for 10 positive plates.

5

Table IL   Properties of Various Substrate Materials

	Substrate Type	Weight ($g/in.^2$)	Thickness (in.)
	Ni plated steel	0.33	0.007
	Electroformed Ni	0.40	0.008
	Electroformed Ni	0.22	0.005
	Perforated Ni	0.25	0.003
20 × 20 mesh	Screen 0.007-in. wire	0.23	0.014
	Screen 0.006-in. wire	0.17	0.012
	Screen 0.005-in. wire	0.13	0.010
	Screen 0.004-in. wire	0.075	0.008
25 × 25 mesh	Screen 0.007-in. wire	0.29	0.014
	Screen 0.006-in. wire	0.21	0.012
	Screen 0.005-in. wire	0.15	0.010
	Screen 0.004-in. wire	0.09	0.008

Table III. Several Plaque Properties

Plaque Thickness (in.)	Plaque Porosity (%)	Plaque Weight $(g/in.^2)$
0.025	78	0.817
0.025	80	0.742
0.025	82	0.668
0.025	84	0.594
0.030	78	0.980
0.030	80	0.890
0.030	82	0.802
0.030	84	0.712
0.035	78	1.142
0.035	80	1.040
0.035	82	0.933
0.035	84	0.839

Table IV. Weight of Active Material

Plate Capacity (Ahr/in.^{2})	Positive Weight (g/in.^{2})	Negative Weight (g/in.^{2})
0.100	0.345	0.273
0.125	0.431	0.341
0.150	0.517	0.410
0.175	0.603	0.477
0.200	0.690	0.546
0.225	0.775	0.615
0.250	0.862	0.673
0.275	0.948	0.751
0.300	1.035	0.817
0.325	1.122	0.887
0.350	1.208	0.956
0.400	1.380	1.090
0.450	1.552	1.225
0.500	1.725	1.360

g. Using these criteria, similar calculations were made for the negative electrode. Flooded negative capacity is based on the positive capacity and factoring in a 1.4:1 negative-to-positive ratio. Therefore:

(27.5-Ahr positive capacity) (1.4) = 38.5 Ahr of flooded negative capacity.

h. At a loading density of 9 Ahr per in.^{3},

$$\frac{38.5 \text{ Ahr}}{9 \text{ Ahr/in.}^3} = 4.28 \text{ in.}^3 \text{ are required}$$

i. Taking the assumption of one more negative plate than positive plate, then 11 negatives are required, or:

$$(11 \text{ negative plates}) \ \frac{(14 \text{ in.}^2)}{\text{plate}} = 154 \text{ in.}^2 \text{ of negative plate.}$$

j. Therefore, the negative plate thickness can be calculated as:

$$\frac{4.28 \text{ in.}^3 \text{ of negative plate}}{1.54 \text{ in.}^2 \text{ of plate area}} = 0.028$$

This value is considered the approximate value for plate thickness.

One factor which has a significant influence on the design of the cell is the plate thickness. As previously mentioned, the value arrived at was influenced by dimensional limitations. However, within these limitations there is some flexibility. In terms of cell weight, it is advantageous to maximize plate thickness since the number of plates will be decreased, thus eliminating some tabs and screen. However, previous studies[2] have shown that by increasing plate thickness, active material is not utilized as efficiently, thus requiring additional material to be present. Also, thicker plates polarized, causing greater voltage drop within the cell. Both effects decrease usable energy density notably as charge and discharge currents increase. It has also been shown that thicker, heavily loaded negative plates do not recombine oxygen as well as thinner plates, which further limits charging and overcharging of cells.

It would then seem that thin plates would produce a cell with better operating characteristics. However, as plates decrease in thickness, they also would have to increase in number, as shown in Table V, in order to provide sufficient cell capacity. Based on substrate weight data (0.005-in., 25×25 mesh), each added plate pair would increase total cell weight by approximately 6 g. On a pro rata basis, this corresponds to 1 Ahr of cell capacity. In other words, to justify a decrease in plate thickness (and add one plate pair), cell capacity would have to be enhanced through greater active material by more than 1 Ahr. These factors were considered in the selection of plate thickness

The other cell components of significance in this design are the electrolyte, cell case, separator, and top assembly. In keeping with earlier discussions concerning the material restrictions of materials exposed to the cell environment, the cell case will be stainless steel. The current-carrying members of the top assembly will be either nickel or stainless steel. The seals used for this design will be of the crimped polymeric type.

The choice of separator material is essentially limited to either nylon or polypropylene. It is believed, based on recent experience well known to aerospace users, that nylon separators have a useful but limited life. Polypropylene separators have been shown to be usable and provide proper plate separation, appears to be resistant to attack by the cell environment, and permit acceptable levels of oxygen recombination. In this context, the use of polypropylene separators was chosen.

The recommended electrolyte is 30% KOH in keeping with the maximum conductivity binary system. Assuming cells will operate in the range of 0 to 20 °C, the addition of lithium or sodium ions to the electrolyte is not expected to have any appreciable effect. Of major importance is the quantity of electrolyte used. Based on data presented in Fig. 1, the quantity of electrolyte will be based on the total pore volume and adjusted to meet the oxygen recombination requirements. The value for the oxygen recombination rate is based on the specific duty cycle and the recombination capabilities of the negative plates. This value for electrolyte quantity is on the order of 80 to 85% of the total pores available.

Using these data and those presented in previous tables, the estimated cell weight is shown in Table VL

10

Table V.   Necessary Plate Thicknesses for Various Numbers of Plates

No. of Plates	Single Plate Area (in.^{2})	Total Plate Area (in.^{2})	*Thickness of Positive Plate (in.)	**Thickness of Negative Plate (in.)
9	14	126	0.031	0.034
10	14	140	0.028	0.030
11	14	154	0.026	0.028
12	14	168	0.023	0.025
13	14	182	0.021	0.024
14	14	196	0.020	0.021
15	14	210	—	0.020

* Based on 3.93 in.^{3} of positive plate

** Based on 4.28 in.^{3} of negative plate

**EFFECTS OF ELECTROLYTE FILL LEVEL
ON CADMIUM IMPREGNATED NI SINTER ELECTRODES**

OXYGEN
RECOMBINATION
RATE

PLATE UTILIZATION
C/2 DISCHARGE RATE

REF. 2,4

DELIVERED CAPACITY – FRACTION OF FLOODED CAPACITY
ALSO RELATIVE OXYGEN RECOMBINATION RATE

FRACTION OF AVAILABLE PORES FILLED WITH ELECTROLYTE
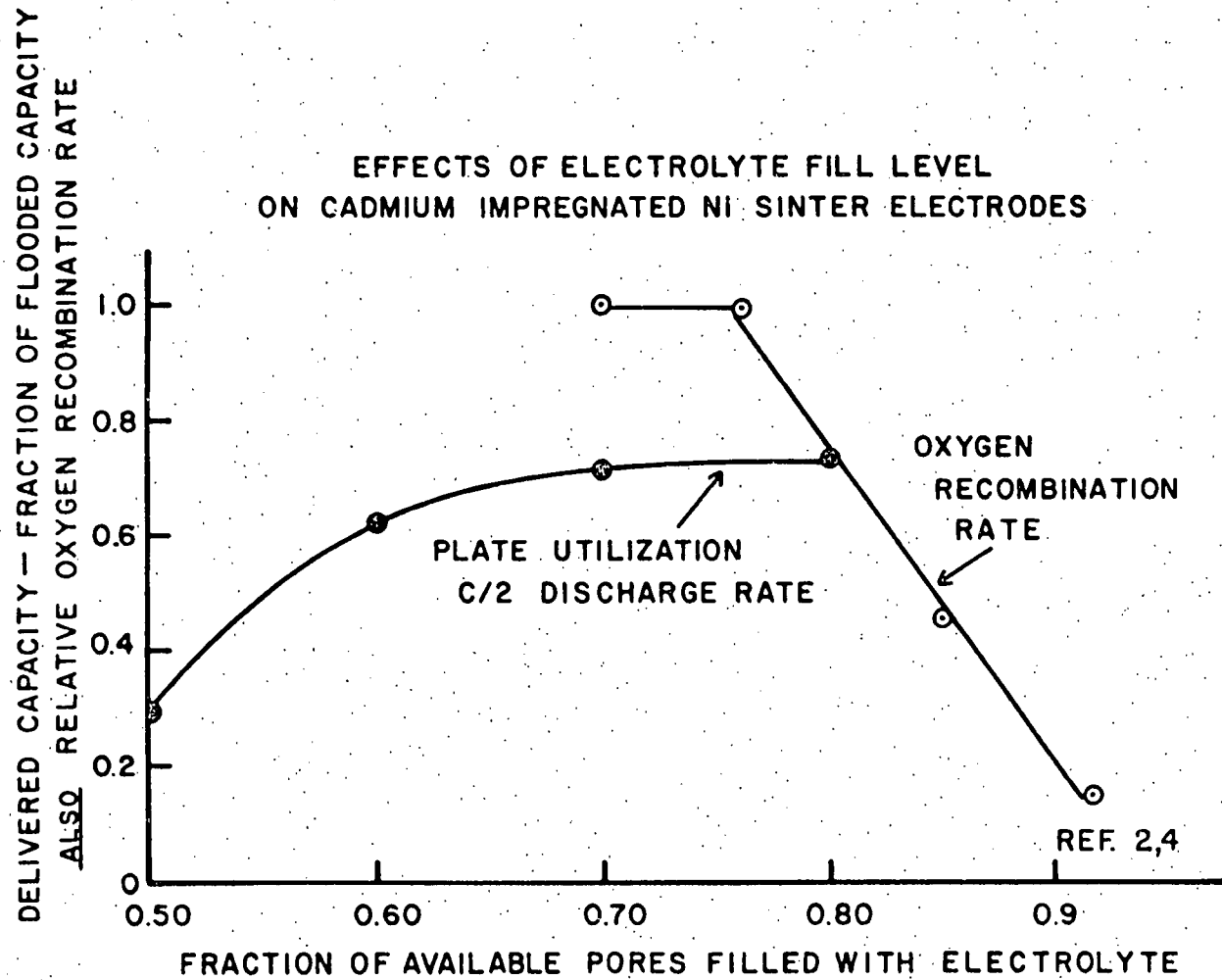
TLI
1/72 EJR

Fig. 1. Effects of electrolyte fill level on cadmium impregnated Ni
sinter electrodes

12

Table VI.   Estimated Cell Component Weight for 20 Ahr Rated Cell

Components	Weight (g)	% Total Weight
Substrate (0.005-in., 25 × 25 mesh)	44	5.6
Plaque (83% porous)	197	25.2
Positive active material	96	12.3
Negative active material	104	13.3
Case	172	22.0
Top assembly, etc.	65	8.3
Separator	11	1.4
Electrolyte	92	11.8
Total	781	100.0

This design would produce a 20-Ahr cell approximately 10% lighter than other 20-Ahr rated cells.

D. Improved Cell Design

   1. 12-Ahr Cell

          When considering the design of the desired 12-Ahr rated cell a similar analysis of an existing aerospace quality Ni-Cd cell was carried out and compared with a proposed cell fitting the physical constraints of the existing cell with the expected improvements incorporated into the design. The calculations are related to those discussed previously for a 20-Ahr rated cell and proceed as follows: the cell is rated at 12-Ahr, and with a 10% safety factor the desired delivered cell capacity will be 13.2 Ahr. This capacity is based on a 1.4 to 1.0 negative to positive capacity ratio operating in the starved condition which is assumed to be at an 80% fill level. Therefore the needed delivered capacities are:

          ● positive capacity - 13.2 Ahr at the 80% fill level the flooded positive capacity would be - 13.2 ÷ 0.8 = 16.5 Ahr

          ● negative capacity - 13.2 × 1.4 = 18.5 A · · at the 80% fill level the flooded negative capacity would be - 18.5 ÷ 0.8 = 23.2 Ahr.

13

These calculations assume 100% efficiency of both the positive and negative electrodes. Given the physical constraints of a typical aerospace 12-Ahr rated cell, the electrode size is selected to be 2.80×3.25 in. or 9.1 in.^{2} If we assume that there will be 10 positive electrodes the total area will be 91.0 in.^{2} and the loading density would be 16.5 Ahr/91.0 in.^{2} or 0.181 Ahr/in.^{2} At a selected electrode thickness of 0.028 in. for positives, the loading per unit volume of plaque would be 6.5 Ahr/in.^{3}, which is within the limits known for positive electrodes. If we assume that there will be 11 negative electrodes, (i.e., one more than positive) the total negative electrode area will be 100.1 in.^{2} and the loading density would be 23.2 Ahr/100 in.^{2} or 0.232 Ahr/in.^{2} At a selected negative electrode thickness of 0.030 in., the loading per unit volume of plaque would be 7.72 Ahr/in.^{3} which again is within known limits for negative electrodes. Such a design will produce a 12 Ahr rated cell with an improved energy density over other cells with the recognized long life capacity ratio.

III. IMPROVED PLAQUE PROPERTY DEVELOPMENT

A. Plaque Properties

A sintered nickel plaque provides the void volume which contains the active material. The porosity of that plaque directly affects the plate capacity. Variations in porosity, therefore, directly affect plate and cell capacity. Consequently, control of the uniformity of plaque porosity and related properties (i.e., pore size distribution, resistance, etc.) is essential for uniform cell behavior. Work reported recently[3] has investigated the manufacturing parameters which affect plaque and plate uniformity. Critical parameters are plaque porosity, pore size distribution, and gauge control. Also, plate loading and gauge control ultimately affect cell uniformity. These variables have been controlled and documented.

Plaque structure can affect the performance of the plate. Thicker,[1,3] less porous structures polarize and/or provide poorer utilization of active material. Both of the effects reduce the energy density of cells and must be minimized through proper selection of plaque structure. These properties of the sintered nickel plaque can be altered by controlled parametric changes in the manufacturing process. Plaque porosity, for example, can be altered by varying the temperature[1,4] of the sintering operation. To properly select a plaque structure, one must also consider the fact that it undergoes changes during the impregnation process. The commonly used chemical impregnation process and the process described by Fleischer can corrode the nickel structure to a degree sufficient to cause sloughing and warping of impregnated plates.[1] These corrosion effects are dependent on the time and temperature of the impregnation process. To compensate, plaques are often made less porous (more dense) in order to withstand the mechanically degrading effects of corrosion. Consequently, plaque structure is not optimized for higher energy density cells.

Another process referred to as the high temperature electrochemical impregnation[5] process affects the sintered nickel plaque to a measurably smaller degree. By virtue of this method, (cathodization in acid nickel or cadmium nitrates), corrosion effects are minimized. This property therefore allows the use of a more open and porous plaque structure without destructive loss of mechanical integrity and electrical conductivity. Since this impregnation method is dependent on the diffusion of ions (H^+, Ni^{+2}, Cd^{+2}) into and (OH^-) out of the plaque, pore structure and surface characteristics[6] are critical properties. Consequently, use of the high temperature impregnation method requires development of a plaque structure not necessarily used with the more conventional impregnation process.

B. Plaque Preparation and Characterization

The production of large quantities of uniform, aerospace quality battery materials suggests the use of manufacturing techniques that allow the close control to those plaque and plate characteristics which affect the final product. Considering the manufacture of plaque, the slurry coating process is inherently easier to control than the dry sintering method. As a result, continuous lengths of slurry-produced plaque can be produced with uniform properties. Initially, short run batch lots of plaque material were produced using the slurry-coating process and the properties of these materials compared to those of dry sinter produced plaque. The plaque produced must not only be lightweight in nature, i.e., have a high porosity and be manufactured on a low weight substrate, but its impregnation characteristics must be such that it allows the necessary loading of active materials to be utilized to the fullest extent.

According to the results of the previous development contract,[3] it was found that the high temperature impregnation method was critically dependent on the physical characteristics of the porous nickel plaque. In fact, it was found that loose dry sinter plaques appeared to deliver higher specific capacities than those plaques manufactured using a slurry coating method. It was suggested that this phenomenon was caused by the formation of a slip-glaze on the surface of the slurry-coated plaque which might narrow the surface pore opening and impede the diffusion processes which necessarily occur during the high temperature impregnation method. This would lead to decreased quantities of active material being deposited within the structure of the plaque and excessive deposits at the plate surface.

16

Obviously, if the optimum plaque material is to be interfaced with the optimum impregnation method, a technique to overcome these apparent shortcomings of the plaque had to be made. During this contract, a successful technique was developed. The pore size distribution of a typical slurry-coated plaque of the type manufactured under the previous contract is indicated in Fig. 2. The distribution was determined on a Micromeritics Model No. 903-1 mercury porosimeter. This shows a large proportion of pores having diameters in two rather distinct regions - 20 to 140 μ and 220 to 340 μ - the majority being in the latter region. When impregnated by the high temperature electrochemical method, this plaque shows an increased thickness due to active material buildup on the surface and poor electrochemical characteristics (i.e., low capacity, after formation due to loss of active material from the surface). In comparison, a typical loose sintered plaque, as shown in Fig. 3, has a well-defined pore size distribution consisting of much smaller pore diameters. When impregnated, this plaque increased in thickness only 0.0014 in. before formation and exhibited a capacity of 7.0 Ahr/in.^{3}, although its other physical properties were similar to that of the previously noted slurry-coated plaque. Attempts to duplicate the pore size characteristics exhibited by loose sintered plaque for slurry-coated material were successful. The slurry formulation and type of nickel powder used were changed (Inco 255 instead of Inco 287) and led to plaque material with pore distribution typified by Fig. 4. It can be seen that the pore diameters are distributed over a range which closely approximates that of the loose sintered type plaque. Investigations into this plaque's loading capabilities indicate substantially increased specific capacities over the earlier slurry coated plaques without appreciable surface buildup.

As discussed previously, uniformity of materials was an important criterion in this contractual effort. Uniformity seems to have been achieved as demonstrated by a slurry-coating run designated TY-8, utilizing 20 × 20 mesh, 0.007 in. nickel wire substrate, and the 255 based slurry. This run provided some 16 feet of plaque material exhibiting the characteristics shown in Fig. 5. Therefore this method of production was used for the fabrication of plaque in this effort.

The effects of varying the sintering conditions of plaque manufactured by the slurry coating process are presented in Table VII on plaque designated as TY-12. It can be seen in the table that, as expected, higher temperatures and longer times at temperature decrease the porosity and gauge of the plaque. It can also be seen that

17
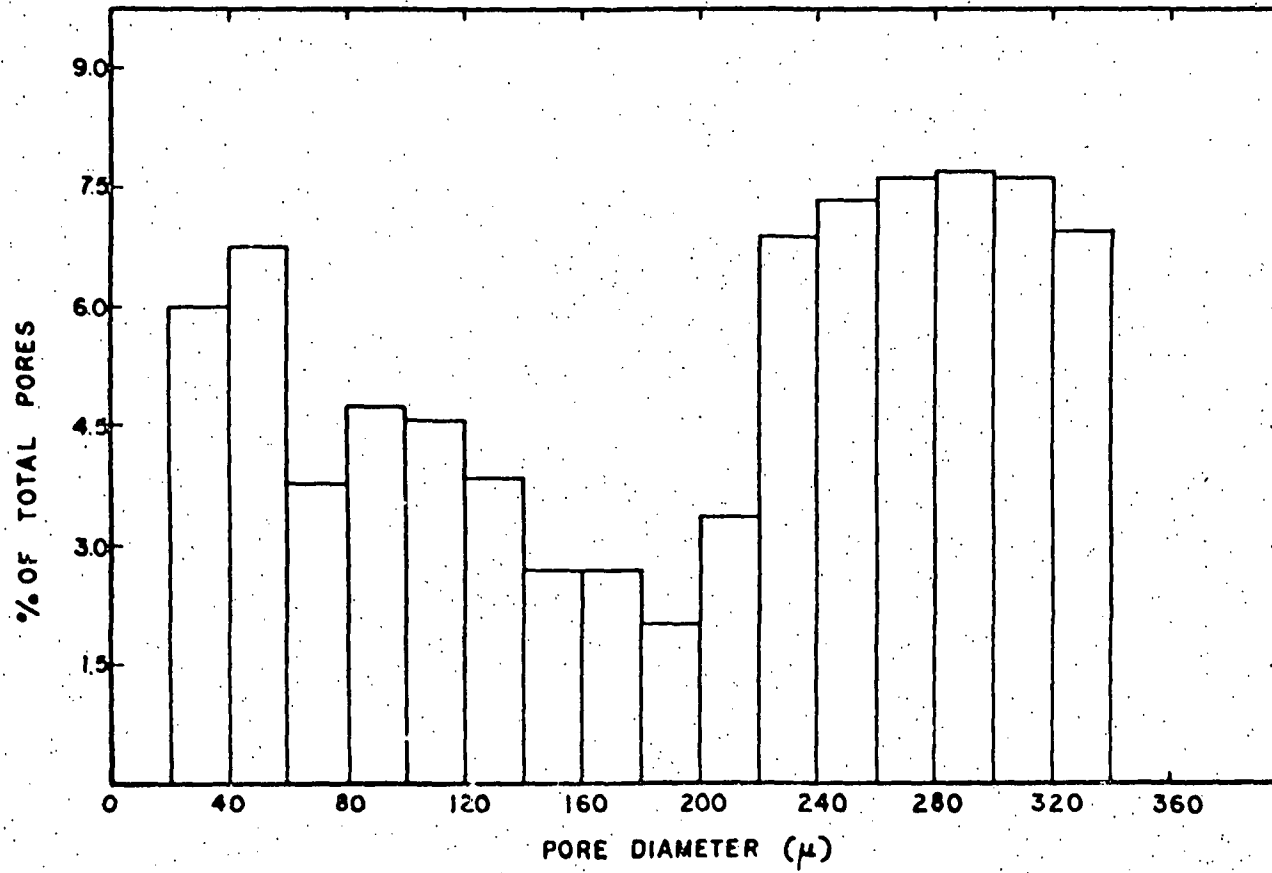
Fig. 2. Typical pore size distribution of "old" formation slurry-coated plaque
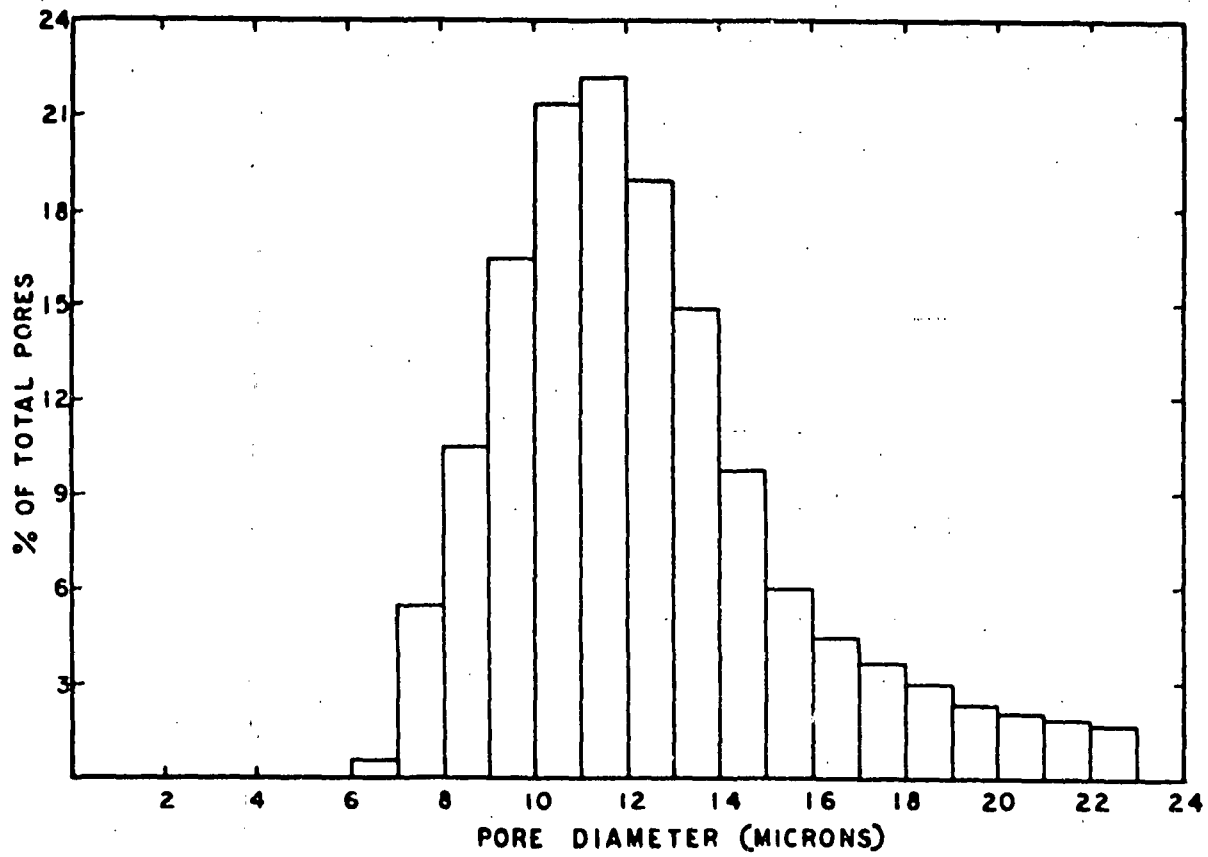
Fig. 3. Typical pore-size distribution of loose Ni sinter plaque
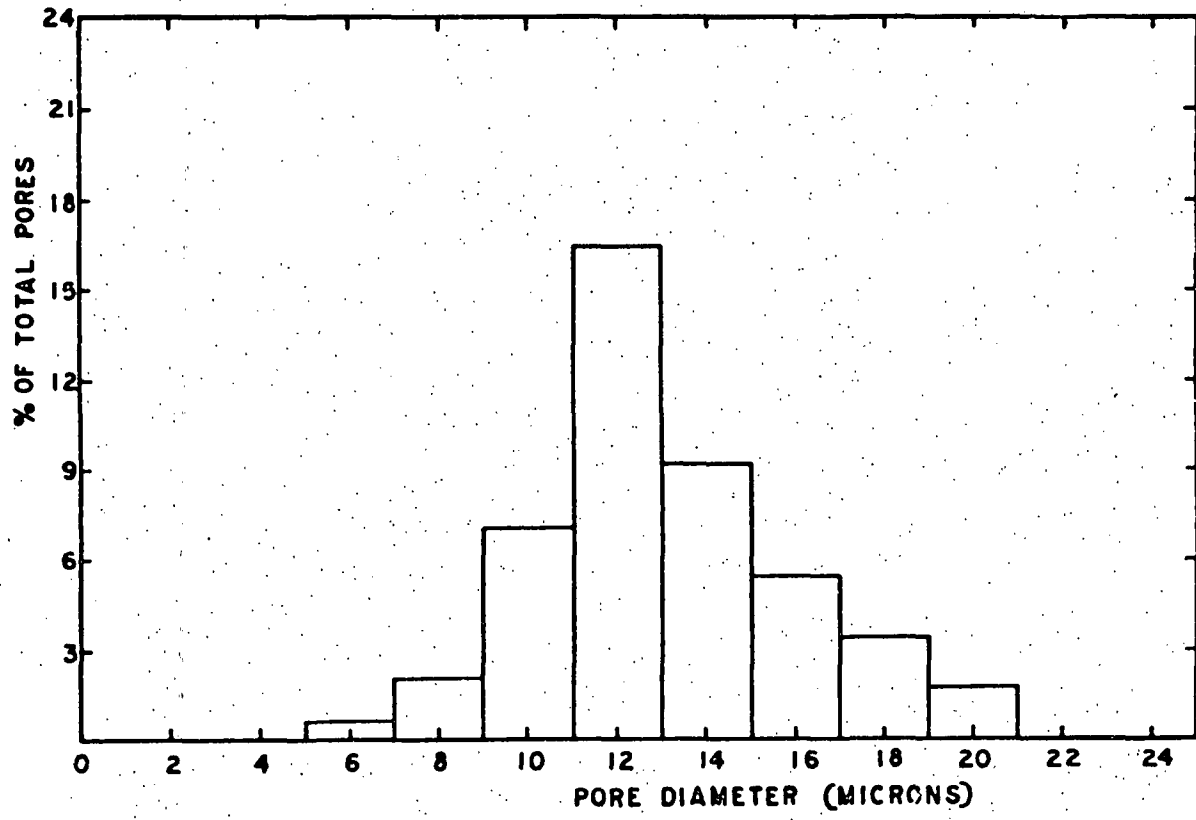
Fig. 4. Typical pore-size distribution of new slurry coated Ni plaque

TYCO NICKEL PLAQUE

TY-8

SINTERED THICKNESS (mils)

APPARENT POROSITY (%)

POWDER POROSITY (%)

WEIGHT/AREA (g/in^2)

SAMPLE NUMBER
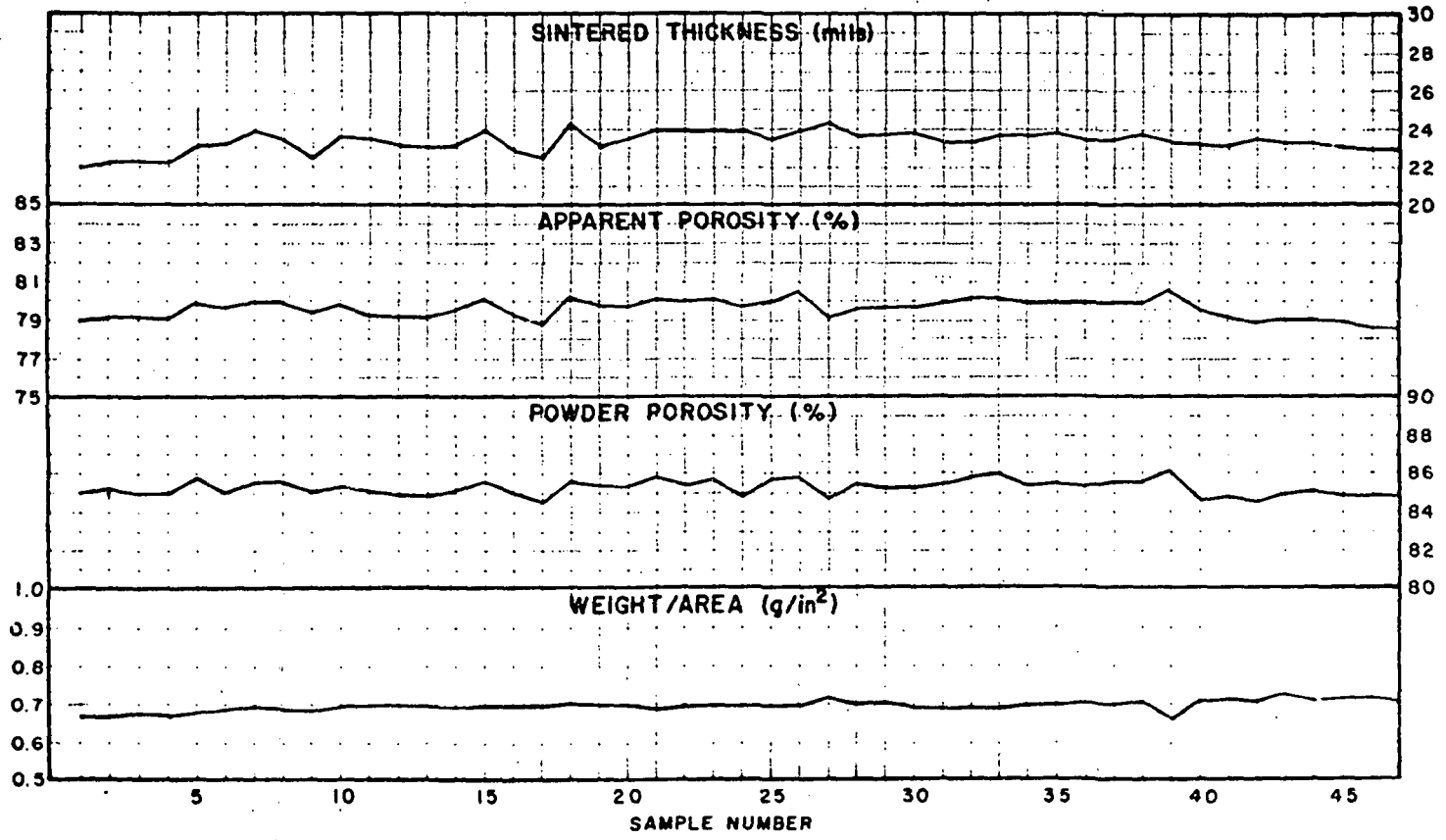
Fig. 5. Uniformity of various properties of new slurry coated Ni plaque

Table VIL   TY-12 Plaque Data

Sinter Time (min)	Plaque Characteristics*	Sinter Temperature (°C)			
		875	900	925	950
15	a			32.7	32.5
	b			1.0323	1.0588
	c			78.4	77.7
	d			82.3	81.6
	e			6.0	5.9
	f			89.3	81.1
20	a		33.5		
	b		1.0268		
	c		79.0		
	d		82.9		
	e		9.4		
	f		47.4		
25	a		32.5		
	b		1.0468		
	c		77.9		
	d		81.8		
	e		6.0		
	f		97.6		
30	a	32.8	31.1	31.4	30.4
	b	1.0610	1.0270	1.0555	1.0451
	c	77.8	77.5	77.0	76.4
	d	81.7	81.7	81.0	80.6
	e	5.7	5.4	5.6	5.3
	f	98.3	97.0	89.2	102.4
40	a	31.7	30.5	30.6	30.1
	b	1.0525	1.0324	1.0452	1.0554
	c	77.2	76.8	76.5	76.0
	d	81.2	80.9	80.9	80.1
	e	5.5	5.2	5.2	5.2
	f	94.7	108.3	107.6	109.3

*a Thickness (mil)
 b Weight (g/in.^{2})
 c Apparent Porosity (%)
 d Powder Porosity (%)
 e Resistivity ($\Omega \cdot$ cm $\times 10^{-4}$)
 f Mechanical Strength (kg/cm^2)

the very short times at lower temperatures has a deleterious effect on the mechanical strength of the plaque. Referring to Table VIII which contains additional data relating to the uniformity of the plaque manufactured for this effort, it should be noted that the large standard deviation found for the mechanical strength measurement may suggest an insensitivity of the test itself when compared to the standard deviations of the other plaque properties. Nonetheless any gross variation in this measurement should still be construed as a real property of the subject material as noted previously.

The substrate used in the manufacture of plaque is purchased from National-Standard Company of Corbin, Kentucky. This material is unique in that the screen is calendered after weaving, which induces cold welding of the wires at their cross-over points. This property further enhances the mechanical stability of the plaque structure and minimizes loose wires and resultant short circuits. Fig. 6 shows a cross sectional view of wire mesh similar to that used in our plaque. The nickel wire is Grade "A" or No. 200. The analysis of this type of wire is as follows:

Nickel + (Cobalt)	99.0	min.
Carbon	0.15	max.
Manganese	0.35	max.
Iron	0.40	max.
Sulphur	0.010	max.
Silicon	0.35	max.
Copper	0.25	max.

The tensile range on 0.005-in. annealed wire is 64,000 to 72,000 psi.

Table VIII. TY-16 Plaque Data

Plaque No.	Sintered Thickness (mils)	Plaque wt - g/in^2 (corrected for substrate)	Apparent Porosity	Powder Porosity	Resistivity $\Omega \cdot cm$	Mechanical Strength (kg/cm^2)
1	29.97	0.73	78.80	82.32	0.006	91.83
2	29.35	0.71	78.05	82.42	0.00612	80.64
3	29.86	0.685	78.98	82.32	0.006	80.81
4	29.45	0.691	78.56	82.94	0.00612	71.32
5	28.77	0.694	78.00	82.45	0.00564	90.80
6	28.86	0.694	78.06	82.51	0.00636	83.78
7	28.95	0.689	78.25	82.69	0.00622	94.93
8	28.51	0.692	77.83	82.32	0.00598	91.77
9	28.90	0.686	78.28	82.73	0.00616	85.99
10	28.73	0.689	78.09	82.55	0.00632	90.56
11	28.72	0.684	78.19	82.63	0.00622	107.19
12	28.57	0.680	78.20	82.70	0.00612	89.35
Mean	29.05	0.693	78.27	82.63	0.00610	88.25
Standard Deviation, σ	0.503	0.0137	0.340	0.283	0.0019	8.87
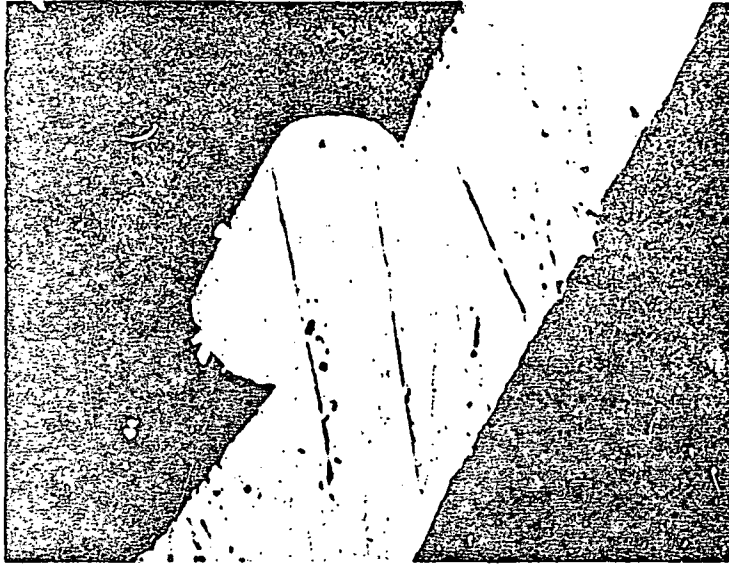
Fig. 6. Cross-sectional view of cold welded nickel wire substrate

IV. IMPROVED PLATE PROPERTY DEVELOPMENT

A. Impregnation Method

A first step in plate production is to determine which impregnation method will be used and what effect it has on plate and cell uniformity and reproducibility.

With regard to plate manufacture, the high temperature electrochemical impregnation method gives the best control of the distribution and morphology of the active materials.

The so-called chemical method and the process described by Fleischer have been used widely in the manufacture of nickel-cadmium electrodes. The relatively new high temperature method referred to above has not been used extensively. It has several notable advantages. Its speed (approximately 1 hr to impregnate plates) is very attractive to manufacturers since cost savings can be realized. The technical advantages are also noteworthy. The fact that electric current is used to precipitate the active material has two important advantages. Firstly, the uniformity of active material is directly related to current distribution over the plaque surface. The use of well-established electroplating methods minimizes any variability. Secondly, the quantity of active material is proportional to the applied current. This provides a direct control over the capacity of a given plate. Other impregnation methods rely solely on the properties of the plaque to effect capacity uniformity. This uniformity within a given plate and from plate to plate is most desirable for high quality cells where cell to cell reproducibility is required. This is especially true where cells are series connected in a battery and subjected to deep depths of discharge. The chance of overdischarge is thereby substantially reduced.

Other notable advantages are the characteristics of cadmium electrodes prepared using the subject impregnation method. The plates show a higher utilization of active material which is an advantage when designing a plate which maximizes

energy density. In addition, these plates show less fading when subjected to repeated cycles[3] (similar to near-earth orbit). The results indicate that a higher energy density and longer lived nickel-cadmium cell are possible through use of this impregnation method.

B. Positive Plate

Initial investigations of the use of the high temperature electrochemical impregnation method focused on its use to manufacture positive plates. Laboratory studies consisted of the impregnation of nickel sinter plaques developed previously in this work in 2 liter beakers containing the various solution compositions. Each plaque was held in a Teflon fixture, parallel to two equidistant platinized titanium counter electrodes on each side of it. Held constant throughout the studies were the following:

1. Solution to plaque area ratio

2. Solution temperature

3. All solutions were freshly prepared, i.e., used within a two hour period of preparation.

Parameters that varied during the study were the following:

1. Current density

2. $Ni(NO_3)_2$ concentration

3. $NaNO_2$ concentration

4. Solution pH

Plaque used in the studies were physically characterized and nominally similar to the originally proposed in the design.

First, in order to gain knowledge leading to the optimum impregnation conditions to be used to obtain positive plates of the type and loading necessary for this program, an impregnation time versus weight gain relationship was generated. Eight plaques from run TY-16 were impregnated for various lengths of time at a current density of 0.5 A/in.[2] Plaque data reported previously appears in Table IX.

In order to glean as much information as possible from these experiments, it was decided to analyze the solutions after every impregnation, each solution being freshly prepared of 2.0 M $Ni(NO_3)_2$ and 0.3 M $NaNO_2$ adjusted to pH 4.0. Also, during

Plaque No.	Sintered Thickness (mils)	Plaque Weight (g. in.^{2})	Apparent Porosity (%)	Powder Porosity (%)	Resistivity (Ω-cm $\times 10^{-4}$)	Mechanical Strength (kg. cm^2)
1	29.9	0.96	78.80	82.32	6.00	91.83
2	29.3	0.94	78.05	82.42	6.12	80.64
3	29.9	0.92	78.98	83.32	6.00	80.51
4	29.4	0.92	78.56	82.94	6.12	71.32
5	28.8	0.92	78.00	82.45	5.64	90.80
6	28.9	0.92	78.06	82.57	6.36	83.78
7	28.9	0.92	78.25	82.69	6.22	94.93
8	28.5	0.92	77.83	82.32	5.98	91.77
9	28.9	0.92	78.28	82.73	6.16	85.99
10	28.7	0.92	78.09	82.55	6.32	90.50
11	26.7	0.92	78.19	82.63	6.22	107.19
12	28.6	0.91	78.20	82.70	6.12	89.35
13	28.9	0.91	78.46	82.92	6.06	81.62
14	28.9	0.91	78.52	82.99	6.40	84.84
15	29.1	0.90	78.34	83.30	6.14	77.28
16	30.3	0.92	79.18	83.47	6.14	85.04
17	28.8	0.89	78.74	83.24	6.58	72.61
18	28.3	0.91	78.05	82.52	6.60	81.53
19	28.2	0.90	78.23	82.79	6.42	95.64
20	28.6	0.90	78.49	83.01	5.98	98.74
21	28.3	0.89	78.37	82.92	6.34	80.44
22	28.4	0.89	78.47	83.01	6.10	84.60
23	28.5	0.89	78.44	82.98	6.54	98.48
24	28.9	0.89	78.74	83.22	6.18	94.49
25	29.4	0.89	79.12	83.55	6.78	77.35
26	28.2	0.89	78.46	83.04	6.40	97.14
27	28.7	0.90	78.55	83.05	6.64	101.64
28	28.9	0.89	78.93	83.43	6.18	94.03
29	28.9	0.90	78.77	83.25	6.16	88.31
30	28.4	0.88	78.45	83.30	6.36	89.10
31	28.2	0.88	78.77	83.36	6.48	91.99
32	27.9	0.88	78.24	82.87	5.92	97.75
33	27.9	0.88	78.27	82.89	6.22	76.93
34	28.6	0.89	78.71	83.23	6.42	84.49
35	28.5	0.89	78.69	83.23	6.66	97.39
36	27.8	0.88	78.24	82.87	6.14	83.96
37	28.0	0.87	78.67	83.30	6.22	91.80
38	28.4	0.89	78.63	83.17	6.32	95.08
39	28.0	0.88	78.48	83.10	6.46	106.64
40	28.0	0.88	78.47	83.09	6.08	100.49
41	28.2	0.87	78.78	83.37	6.48	85.86
42	28.4	0.88	78.74	83.30	6.58	93.57
43	28.2	0.88	78.59	83.17	6.50	85.62
44	28.2	0.89	78.40	82.92	6.56	90.90
45	28.1	0.88	78.63	83.23	6.28	87.04
46	28.2	0.88	78.67	83.26	6.46	101.90
47	28.2	0.88	78.66	83.25	6.66	91.53
48	27.8	0.88	78.38	83.02	6.28	91.65
49	27.7	0.87	78.56	83.23	6.42	73.49
50	28.0	0.87	78.79	83.43	6.66	92.37
51	28.1	0.86	79.06	83.70	6.76	91.06
52	27.6	0.87	78.28	82.95	5.80	84.77
53	27.8	0.89	78.08	82.71	6.04	91.91
54	28.0	0.87	78.65	83.28	6.86	96.89
55	27.0	0.86	78.25	83 03	6.80	108.90
56	27.1	0.85	78.61	83.39	6.28	110.63

Table IX. TY-16 Plaque Characteristics

29

the longest time run, the change in pH at temperature was monitored as was the change in plaque potential versus an Ag/AgCl reference electrode. The results are presented graphically in Fig. 7. It is interesting to note that TY-16-7, the 75-min impregnation in Fig. 12 which showed no buildup of material in its surface, roughly coincides with a sharp potential break, a slight decrease in the solution pH, and the approximate demise of nitrite ion from the solution. Metallographic sections of these plaques showed the TY-16-7 plaque to be uniformly filled with active material. Plaques with shorter impregnation times were uniform but not completely filled, and plaques impregnated for longer times began to accumulate active material on their surfaces, although the pore structure was uniformly filled. The potential break is probably associated with the loss of nitrite ion from the solution and subsequent loss of pH control. Photographs of cross sections of all plates are shown in Figs. 8 through 15.

A few words should be mentioned about the analyses of the impregnation baths. Reproducibility of analyses was excellent where tested. Most solutions were analyzed for Ni^{++}, $NaNO_2$, and total nitrogen concentration. The data are shown in Table X. These results suggest the trends in the chemistry of the high temperature electrochemical impregnation method.

On the basis of a 2.0 M $Ni(NO_3)_2$, 0.3 M $NaNO_2$ solution, this will contain 60.2 g/ℓ nitrogen theoretically. Looking at Table X, therefore, the difference between the total theoretical nitrogen and the measured total nitrogen gives an indication of the amount of nitrogen lost either on heating or during the impregnation process (as NO_x). Similarly, the difference between the measured total nitrogen and the total due to $Ni(NO_3)_2$ and $NaNO_2$ combined gives an indication of the amount of $NaNO_3$ formed (should be inversely proportional to $NaNO_2$ concentration). This decrease in $NaNO_2$ concentration should then have an effect on the solution pH.

Further investigation of the positive electrode impregnation regime continued with variations in the chemical composition and current density. The results are summarized in Tables XI, XII, and XIII. The main conclusion to be drawn from these data is that the operating conditions (on a laboratory scale) for the impregnation of positive plates [2.0 M $Ni(NO_3)_2$, 0.3 M $NaNO_2$, pH 4.0, 105°C, 0.5 A/in.^{2}, 75 min] produced electrodes with acceptable weight gain. The delivered capacity of the plates is recorded in the above-mentioned Tables. Table XIV summarizes the capacity data found in the previous three tables presented along with active material utilizations. In general, the uniform plate efficiencies suggest an agreement between the plaque properties of TY-16 and the utilization of active material found in these plaques.

30
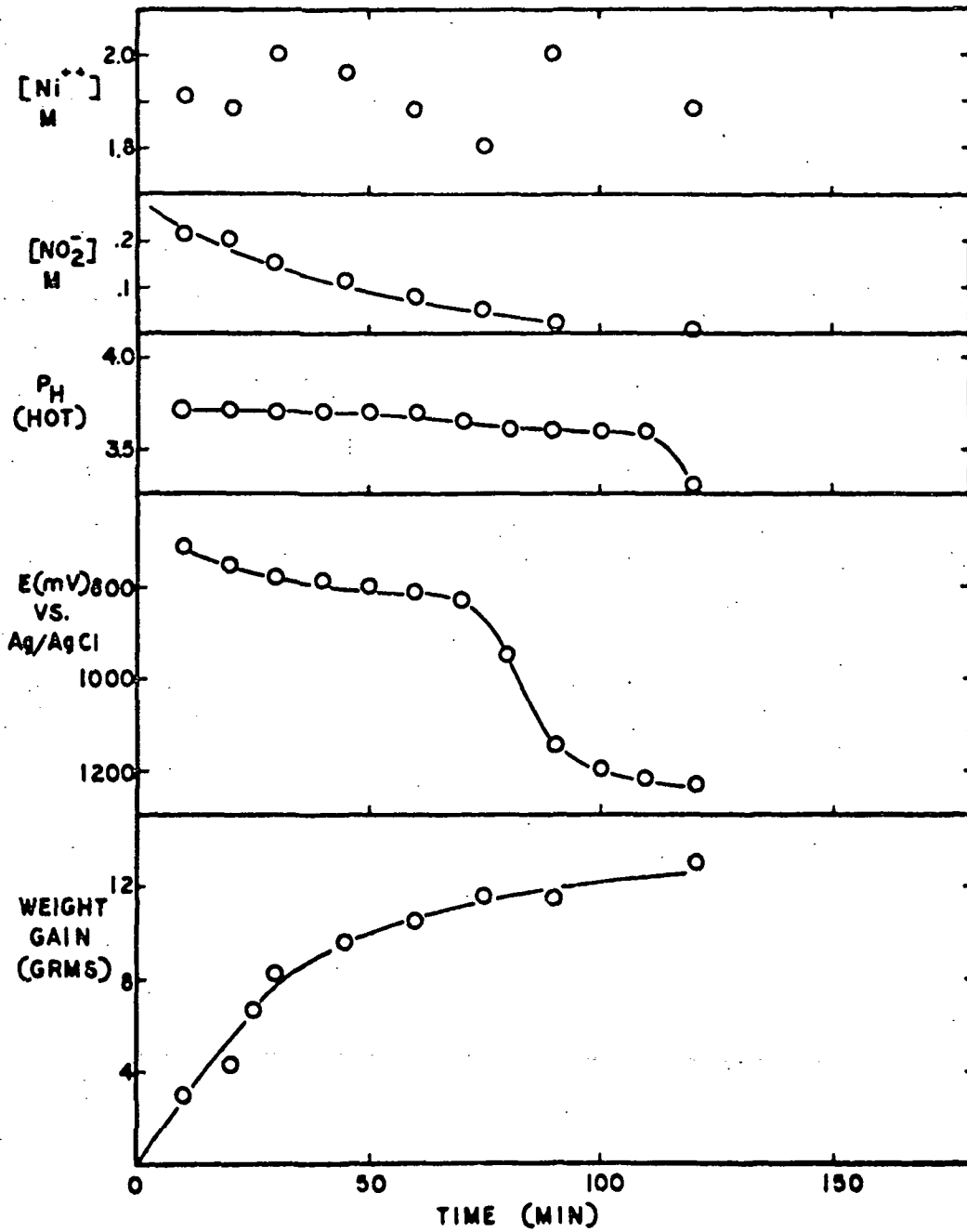
Fig. 7. Slurry run TY-16 impregnation study data
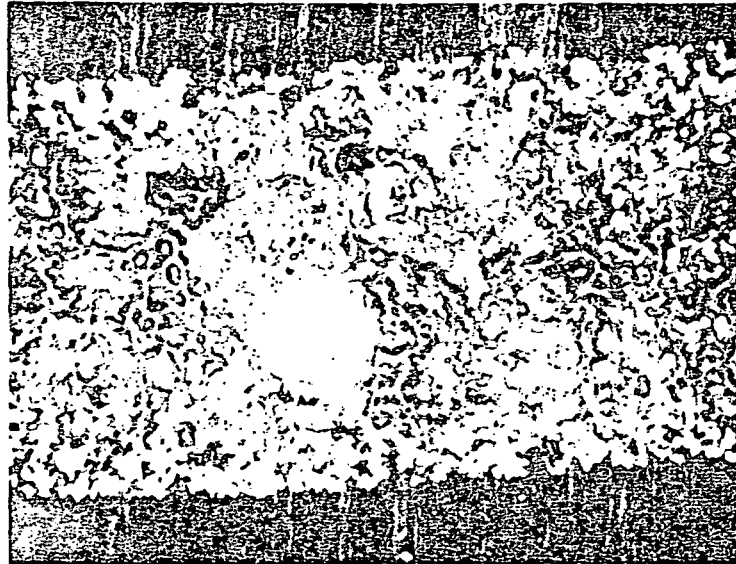
Fig. 8. TY-16-1 - 10 minute impregnation (90 X)

Fig. 9. TY-16-2 - 20 minute impregnation (90 X)

Fig. 10. TY-16-4 - 30 minute impregnation (90 X)
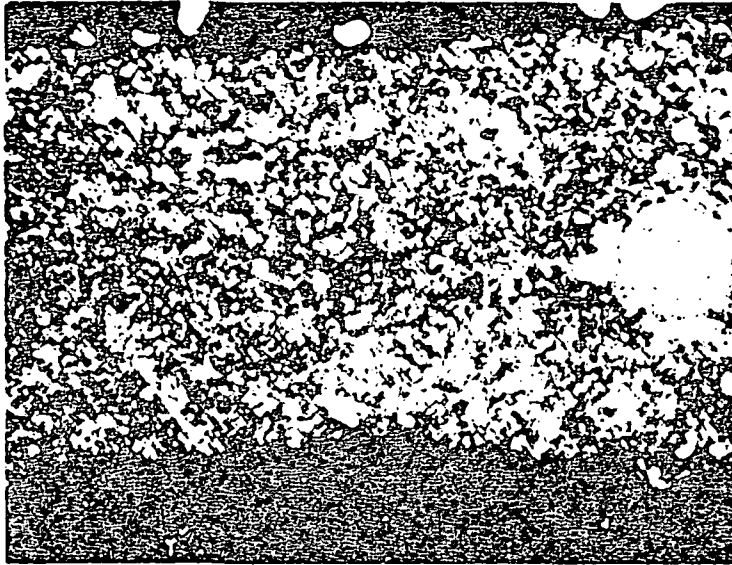
Fig. 11. TY-16-5 - 45 minute impregnation (90 X)

35
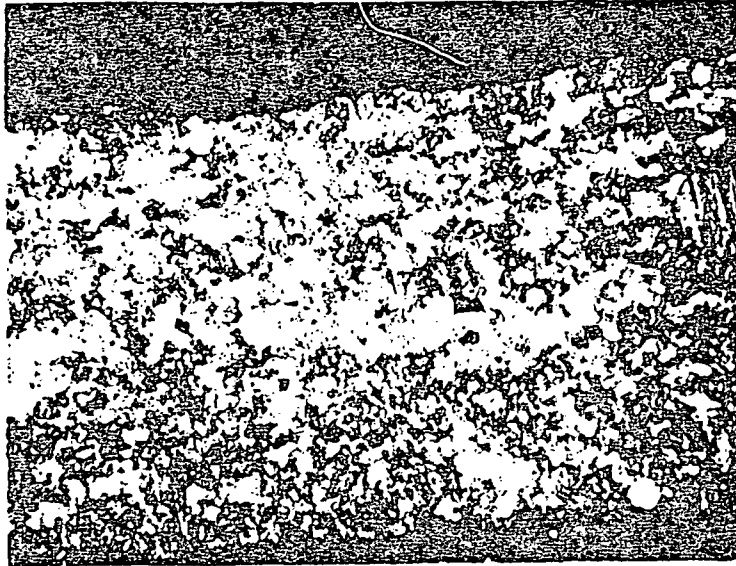
Fig. 12. TY-16-6 - 60 minute impregnation (90 X)

Fig. 13. TY-16-7 - 75 minute impregnation (90 X)
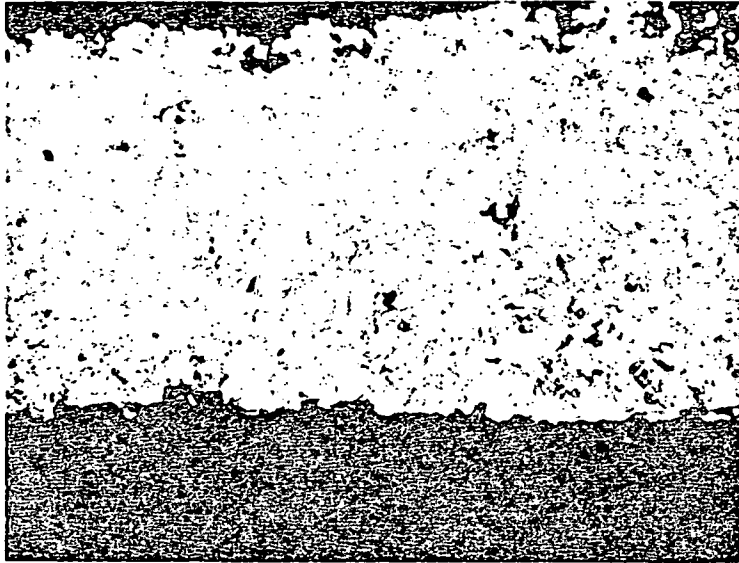
Fig. 14. TY-16-10 - 90 minute impregnation (90 X)

Fig. 15. TY-16-8 - 120 minute impregnation (90 X)

Table X. TY-16 Chemical Analysis Data

Impregnation Time (min)	Ni(NO3)2 Molarity	g/ℓ (N)	NaNO2 Molarity	g/ℓ (N)	Total Nitrogen g/ℓ Measured	Calculated
10	1.909	53.45	0.2049	2.87	56.2	56.32
20	1.879	52.61	0.2016	2.82	55.1	55.43
30	2.00	56.00	0.147	2.06	57.96	58.06
45	1.96	54.88	0.1156	1.62	57.26	56.50
60	1.88	52.64	0.0726	1.02	55.86	53.66
75	2.08	50.40	0.0504	0.706	55.30	51.11
90	2.08	58.24	0.0216	0.30	60.05	58.54
120	1.88	52.64	0.00	0.00	53.27	52.64

Table XI Effect of $Ni(NO_3)_2$ Concentration*

Plaque No.	Plaque Thickness (mils)	Plate Thickness (mils)	Plate after Formation (mils)	Ni(NO3)2 Conc. (M)	Theoretical Plate Capacity (Ahr)	Delivered Capacity (Ahr)	Final NO2⁻ Conc. (M)	Final pH
TY-16-23	28.5	31.5	31.3	1.75	3.24	3.22	0.092	5.65
TY-16-25	29.4	31.5	31.5	1.90	3.22	3.17	0.083	5.58
TY-16-18	28.3	31.8	31.3	2.00	3.41	3.03	0.078	5.42
TY-16-19	28.3	30.2	29.3	2.50	3.00	2.64	0.074	5.16
TY-16-20	28.6	30.1	28.7	3.00	2.59	2.31	0.056	5.57

*All experiments were run on 16-in.^{2} electrodes for 75 min at 0.5 A/in.^{2} The solutions contained 0.3 M $NaNO_2$, adjusted to pH 4.0, and were maintained at their boiling point.

Table XII   Effect of NaNO$_2$ Concentration at Various Ni(NO$_3$)$_2$ Concentrations*

Plaque No.	Plaque Thickness (mils)	Plate Thickness (mils)	Plate after Formation (mils)	Ni(NO$_3$)$_2$ Conc. (M)	NaNO$_2$ Conc. (M)	Theoretical Plate Capacity (Ahr)	Delivered Capacity (Ahr)	Final NO$_2$ Conc. (M)	Final pH
TY-16-12	28.6	30.5	29.4	2.00	0.0	3.15	2.50	–	0.3
TY-16-11	28.7	30.9	30.0	2.00	0.0	2.92	2.94	–	0.6
TY-16-9	28.9	30.3	30.3	2.00	0.0	3.07	3.05	–	0.4
TY-16-30	28.4	29.2	29.0	2.00	0.2	2.96	2.79	0.0165	4.78
TY-16-18	28.3	31.8	31.3	2.00	0.3	3.41	3.03	0.078	5.42
TY-16-28	28.9	34.6	29.8	1.75	0.6†	3.00	2.26	0.147	4.80
TY-16-27	28.7	33.9	31.4	2.00	0.6†	3.36	3.31	0.15	5.11
TY-16-26	28.2	31.0	30.7	2.50	0.6†	3.26	3.20	0.17	5.18
TY-16-29	28.9	30.7	29.8	3.00	0.6†	3.16	2.43	0.147	4.46

†Gross active material precipitation occurred in the bath at this concentration.

*All experiments were run on 16-in.^{2} electrodes for 75 min at 0.5 A/in.^{2} The solutions were all adjusted to pH 4.0 and maintained at the boiling point.

Table XIII Effect of Current Density Variations*

Plaque No.	Plaque Thickness (mils)	Plate Thickness (mils)	Plate after Formation (mils)	Impregnation Time (min)	Current Density ($A/in.^2$)	Theoretical Plate Capacity (Ahr)	Delivered Capacity (Ahr)	Final NO_2^- Conc. (M)	Final pH
TY-16-31	28.2	30.0	29.2	93.75	0.4	3.35	3.31	0.048	5.25
TY-16-18	28.3	31.8	31.3	75	0.5	3.41	3.03	0.078	5.42
TY-16-34	28.6	31.1	30.1	62.5	0.6	3.35	3.20	0.083	4.51
TY-16-35	28.5	31.0	30.1	53.5	0.7	3.24	3.13	0.104	4.55

*All experiments were run on 16-in.^{2} electrodes in solutions of 2.0 M $Ni(NO_3)_2$ and 0.3 M $NaNO_2$ adjusted to pH 4.0 and maintained at the boiling point. The coulombic input was kept constant in order to be able to compare the finished plates.

Table XIV. Positive Plate Capacity Data*

Plaque No.	Theoretical Capacity	Delivered Capacity	Theoretical Capacity	% Efficiency (revised)	Capacity (Ahr/in.^{3})
TY-16-9	3.07	3.05	2.90	105	6.29
-11	2.92	2.94	2.30	128	6.12
-12	3.15	2.50	2.45	102	5.31
-18	3.41	3.03	3.09	98	6.05
-19	3.00	2.64	2.46	108	5.63
-20	2.59	2.31	2.09	110	5.03
-23	3.24	3.22	3.11	104	6.43
-25	3.22	3.17	3.10	102	6.21
-26	3.26	3.20	2.96	108	6.51
-27	3.36	3.31	3.05	108	6.59
-28	3.00	2.26	2.46	92	4.74
-29	3.16	2.43	2.56	95	5.10
-30	2.96	2.79	2.61	107	6.01
-31	3.35	3.31	2.98	110	7.11
-34	3.35	3.20	2.96	108	6.64
-35	3.24	3.13	2.91	108	6.50
-52	3.00	3.05	2.78	109	6.20
-53	3.05	3.05	2.73	111	6.20
-55	3.00	3.00	2.74	109	6.33

*Plates manufactured under a variety of bath compositions and operating conditions.

These data were obtained by forming the plates flooded in 30% KOH for a minimum of three full cycles (100% overcharge and complete discharge to 0.6 V) at the C/2 rate using oversize negative counter electrodes. The positive plates were then washed, scrubbed, dried, weighed, and retested at the C/2 rate (100% overcharge, complete discharge) in 30% KOH once again. From the table it can be seen that the average revised theoretical capacity is almost 90% of the initial theoretical capacity and that the average delivered capacity is over 100% of the revised theoretical capacity. Listed in Table XIV are plaque numbers TY-16-52, 53, and 55 which were impregnated using the standard solution composition of 2.0 M $Ni(NO_3)_2$, 0.3 M $NaNO_2$, pH 4.0, 105°C and run for 75 min at 0.5 A/in.^{2}, with the addition of 0.1 M $Co(NO_3)_2$. This addition is now part of the standard bath composition used to manufacture positive plates for this contract.[6]

The following are the studies' conclusions:

1. Effect of nickel concentration

a. Delivered capacities are highest at the lower Ni concentrations (~2.0 M) - less active material loss.

b. Plate thickness increases are minimal at higher Ni concentrations (~3.0 M).

c. Nitrite ion consumption increases at higher Ni concentrations.

2. Effect of $NaNO_2$ concentration

a. Higher nitrite concentrations cause gross active material precipitation in the impregnation bath.

b. Higher nitrite appears to cause greater active material loss upon formation of plates.

c. Nitrite concentrations of 0.3 M or less have no effect on delivered capacity.

3. Effect of current density

a. Higher current densities (~1.0 A/in.^{2}) lead to lower capacities - less efficient impregnation - active material precipitation in the bath.

b. Current densities between 0.4 and 0.7 A/in.^{2} have no adverse effect on capacity or final plate thickness.

C. Negative Plate

Initial investigations made toward the selection of an optimized high temperature electrochemical impregnation regime for the negative plate considered in our proposed cell design utilized a number of samples of uniform plaque material from run TY-16, previously used during the optimization of the impregnation method for positive plates. These were physically characterized and then impregnated for various times. The conditions of impregnation consisted of the cathodic precipitation in a freshly prepared solution of 2.0 M $Cd(NO_3)_2$ and 0.3 M $NaNO_2$ adjusted to pH 3.0 at the boiling point of the solution, approximately 105°C. The current density was 0.31 $A/in.^2$ After each impregnation, the solutions were analyzed for chemical content. The change in solution pH and the electrode potential versus a Ag/AgCl reference electrode was also monitored. These data are presented in Fig. 16. The physical appearance of the impregnated plates was very good, with no active material visible on the surface of the plaque until the 60-min run, which also exhibited a plate thickness gain of approximately 4 mils.

Plaque and plate thickness data are presented in Table XV. Increased impregnation periods produced the dendritic growth of active material on the plaque surface. The results of the chemical analysis are presented in Table XVI.

These data again suggest the amounts of nitrogen containing gases evolved and $NaNO_3$ formed during impregnation. Further examination of the data in Fig. 16 shows a dissimilarity of the electrode potential when compared to that of the positive electrode during impregnation and, more strikingly, a less pronounced utilization of the nitrite ion in solution, which is due in part to the decreased current density and impregnation time used. This factor potentially leads to better pH control during the negative impregnation process.

A potential problem involved with the impregnation of Ni plaque to produce negative plate was uncovered during this investigation. It had been assumed that during the high temperature impregnation process, the plaque material is cathodically protected from chemical corrosion in the bath. It was found that after each impregnation, the solution was colored a light green color and Ni ion was immediately suspected. Obviously, in a laboratory scale process where contaminated solutions can be discarded or treated, minute quantities of unwanted materials can be tolerated, but on a large production scale the constant use of such solutions without expensive treatment would eventually lead to co-precipitation of $Cd(OH)_2$ and $Ni(OH)_2$ in the negative plate. It appears that the nickel concentration increases with time in the solution, as shown in Table XVII.

45
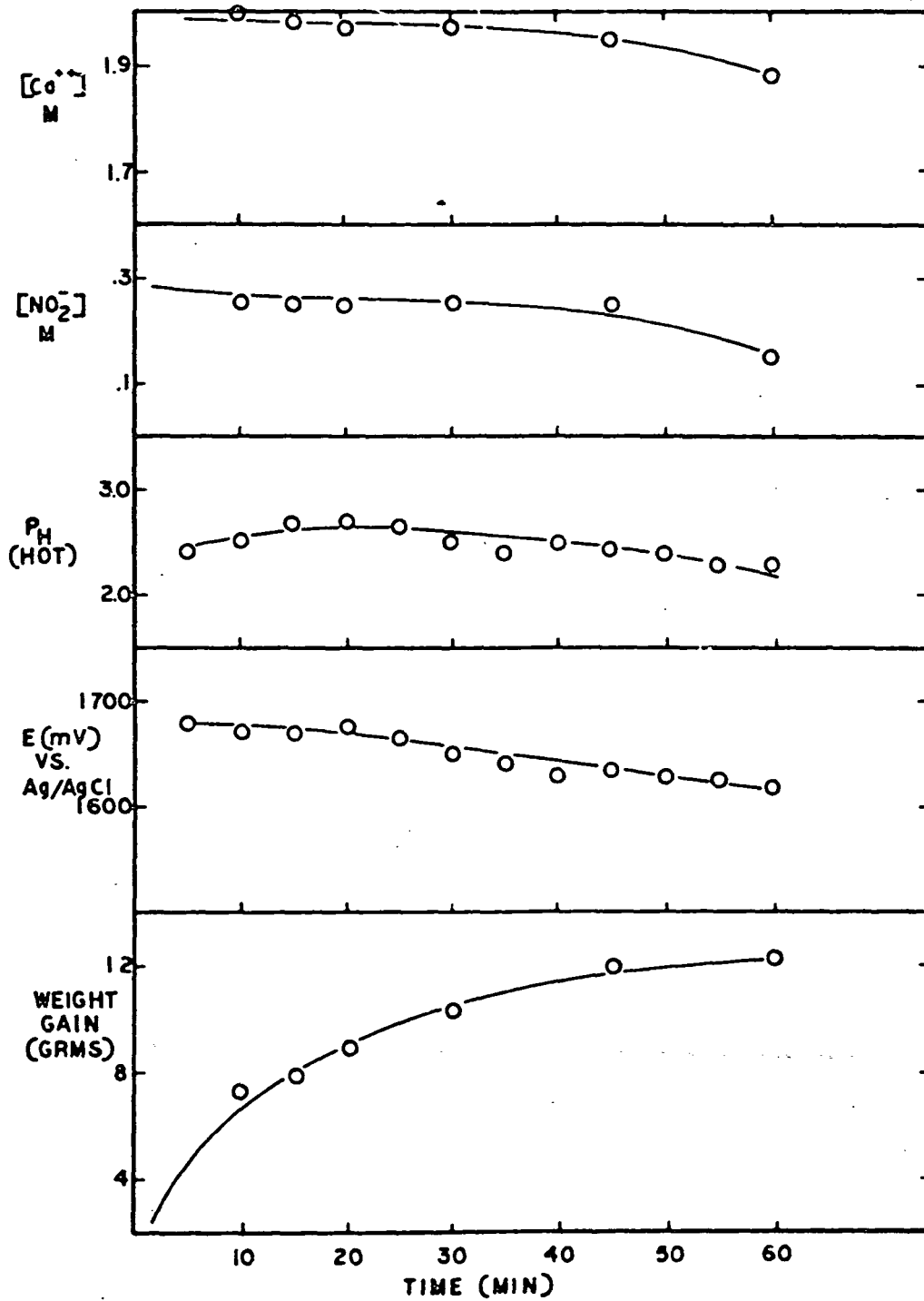
Fig. 16. Negative impregnation study

Table XV. Negative Electrode Thickness Data

Electrode No.	Impregnation Time (min)	Plaque Thickness (mils)	Plate Thickness (mils)
TY-16-13	10	28.9	29.3
-14	15	28.9	29.1
-15	20	29.1	30.7
-17	30	28.8	29.6
-21	45	28.3	30.0
-22	60	28.4	32.6

Table XVL Chemical Analysis of Negative Impregnation Baths

Plaque No. TY-16	Impregnation Time (min)	$Cd(NO_3)_2$ Conc. (M)	N (g/ℓ)	$NaNO_2$ Conc. (M)	N (g/ℓ)	Total Measured	mg/ℓ Calc.
13	10	2.00	56.00	.25	3.50	60.76	59.50
14	15	1.98	55.44	.25	3.50	59.64	58.94
15	20	1.97	55.16	.25	3.50	59.02	58.66
17	30	1.98	55.44	.25	3.50	59.64	58.94
21	45	1.99	55.72	.25	3.50	60.20	59.22
22	60	1.88	52.64	.18	2.52	56.84	55.16

Total theoretical N, 60.2 g/ℓ

Table XVIL Ni Ion Concentration in Cd Impregnation Solutions

Plate No.	Impregnation Time	Ni Concentration (mg/ℓ)
TY-16-13	10	115
-14	15	113
-15	20	140
-17	30	115
-21	45	175
-22	60	172

Obviously, if plaque corrosion is occurring, the best solution is to attempt to avoid or limit it rather than to treat the affected solutions. Treatment of impregnation baths is possible but is time consuming and not totally satisfactory. A chemical, 4-methylnioxime, will selectively precipitate nickel ion from cadmium solutions at pH 3.0 [as opposed to dimethylglyoxime, which must work at pH 10 and would, of course, also precipitate $Cd(OH)_2$]. This is not only expensive, but if excess amounts are left in the bath, it may precipitate out in the next nickel plaque to be impregnated. Finally, the effects of such an organic material in the bath are totally unknown.

A more optimistic approach involves the light oxidation of the nickel plaque (heating in air) prior to impregnation which appears to inhibit corrosion and yet not adversely affect the electrical or physical properties of the plaque. Plaque was treated in this manner prior to impregnation in the bath mentioned above at 0.31 $A/in.^2$ for 25 min. Their thickness data is exhibited in Table XVIII. It can be seen from these data that the thickness increase upon impregnation is but a few tenths of a mil. Under identical impregnation conditions the nickel content of the cadmium solutions after impregnation of passivated plaque was less than 0.5 mg/ℓ, whereas plaques impregnated without passivation have shown nickel contamination up to 175 mg/ℓ. In addition to the prevention of plaque corrosion, the passivation minimizes any buildup of active material on the outside of the plaque. Negative plate utilization was found to be substantially lower, on the order of 80% of the revised theoretical capacity, i.e., the plate capacity based on the weight of active material in the plate after formation. Therefore, the projected design capacity for the negative electrode had to be projected upward to maintain the proper positive to negative capacity ratio.

After a thorough investigation of the parameters involved in the manufacture of negative plate material by the high temperature electrochemical method, a procedure for its production was selected. The optimum conditions were impregnation of the plaque material in a bath consisting of $Cd(NO_3)_2$ at a concentration between 2.0 and 3.0 M and a $NaNO_2$ concentration sufficient to maintain the solution pH between 2.0 and 3.0 (typically 0.3 M). The bath temperature should be maintained at the boiling point (105°C) and impregnation should be carried out at a current density of 0.5 $A/in.^2$ Impregnation of properly treated plaque (of nominal 83% porosity) was carried out at this current density for up to 40 min without undue plate thickness increases. These conditions were selected based on data presented in Tables XIX, XX, and XXI. In Table XIX it can be seen that $Cd(NO_3)_2$ concentrations below 2.0 M tended to produce

48

Table XVIII Negative Plate Data - TY-18

Plate No.	Initial Thickness (mils)	Final Thickness (mils)	Thickness Change (mils)
1	30.6	30.7	+0.1
2	30.7	30.9	+0.2
3	30.7	31.0	+0.3
4	31.0	31.1	+0.1
5	29.8	30.2	+0.4
6	30.8	31.1	+0.3
7	31.5	31.5	0.0
8	31.4	31.7	+0.3
9	29.6	30.0	+0.4
10	29.8	29.7	- 0.1
11	29.7	30.2	+0.5
12	30.7	30.9	+0.2
13	29.5	29.5	0.0
14	29.6	30.0	+0.4
15	20.0	30.1	+0.1
16	30.1	30.5	+0.4
17	30.5	31.0	+0.5
18	30.0	30.5	+0.5
19	30.3	30.8	+0.5
20	30.4	30.5	+0.1

Table XIX. Effect of $Cd(NO_3)_2$ Concentration on Negative Electrodes[*]

TY-18 Plaque Number	Plaque Thickness (mils)	Plate Thickness (mils)	Plate After Formation Thickness (mils)	$Cd(NO_3)_2$ Concentration (M)	Theoretical Capacity	Revised Theoretical Capacity	Delivered Capacity	Plate Capacity ($Ahr/in.^3$)
57	29.2	37.1	35.5	2.0	5.75	5.05	4.06	7.15
59	29.3	37.6	35.7	2.0	5.85	5.11	4.06	7.11
38	30.7	31.2	30.8	2.0	6.02	5.07	3.93	7.97
42	30.4	31.4	30.7	2.0	5.82	5.01	4.03	8.20
87	29.8	37.1	33.2	3.0	6.16	4.89	4.20	7.91
88	30.4	31.9	31.1	2.5	6.18	4.92	4.30	8.64
86	30.8	31.1	31.4	1.75	4.88	4.08	3.20	6.37
85	30.7	31.2	30.9	1.75	4.61	3.78	2.93	5.93
98	30.8	34.8	-	1.5	4.49	-	-	-

[*] Constant $0.3M$ $NaNO_2$, $0.5 A/in.^2$, 35 min.

Table XX. Effect of NaNO$_2$ Concentration on Negative Plates*

TY-18 Plaque Number	Plaque Thickness (mils)	Plate Thickness (mils)	Plate After Formation Thickness (mils)	NaNO$_2$ Concentration (M)	Theoretical Capacity	Revised Theoretical Capacity	Delivered Capacity	Plate Capacity (Ahr/in.^{3})
37	29.9	30.3	30.4	0.0	4.27	3.54	2.93	6.04
57	29.2	37.1	35.5	0.3	5.75	5.05	4.06	7.15
59	29.3	37.6	35.7	0.3	5.85	5.11	4.06	7.11
38	30.7	31.6	30.8	0.3	6.02	5.07	3.93	7.97
42	30.4	31.4	30.7	0.3	5.82	5.01	4.03	8.20
41	29.8	30.8	30.3	0.6	5.55	4.72	3.60	7.43

* Constant 2.0M Cd(NO$_3$)$_2$, 0.5 A/in.^{2}, 35 min.

Table XXI. Effect of Current Density on Negative Plates*

TY-18 Plaque Number	Plaque Thickness (mils)	Plate Thickness (mils)	Plate After Formation Thickness (mils)	Impregnation Time (min)	Current Density (A/in.^{2})	Theoretical Capacity	Revised Theoretical Capacity	Delivered Capacity	Plate Capacity (Ahr/in.^{3})
38	30.7	31.6	30.8	35.0	0.5	6.02	5.07	3.93	7.97
42	30.4	31.4	30.7	35.0	0.5	5.82	5.01	4.03	8.20
57	29.2	37.1	35.5	35.0	0.5	5.75	5.05	4.06	7.15
59	29.3	37.6	35.7	35.0	0.5	5.85	5.11	4.06	7.11
79	30.9	33.0	32.8	23.5	0.75	5.05	4.13	3.93	6.54
81	30.5	36.2	35.3	17.5	1.00	5.69	4.69	3.73	6.60

* Constant 2.0M Cd(NO$_3$)$_2$, 0.3M NaNO$_2$

plates of somewhat lower capacity than those impregnated in concentrations of 2.0 M or above. Table XX illustrates that the necessary pH control is maintained at values of 0.3 M $NaNO_2$. Higher values serve no purpose while lower values invite unacceptable levels of nickel concentration into the cadmium solution via excessive plaque corrosion.

Experiments involving nitrite ion concentration have shown that even with passivated plaque, corrosion of the plaque will occur if no $NaNO_2$ is included in the bath formation. Nickel concentrations as high as 50 mg/ℓ were found after 35 min at 0.5 A/in.^{2} current density in such solutions as opposed to concentrations of < 0.5 mg/ℓ in baths in which the pH was controlled with nitrite concentrations of approximately 0.3 M.

For a given coulombic input, the effect of increasing current density is to decrease the theoretical and delivered capacity of the negative plate. as shown in Table XXL Current densities of lower value, although not listed in the table, suggest a decreased plate capacity also.

D. Plate Testing

Study of the electrochemical performance characteristics in the flooded condition of both positive and negative plates manufactured by the optimum conditions previously discussed was initiated. This was done by testing five positive and five negative electrodes in a simulated near-earth orbit cycle regime at a charge-discharge rate corresponding to a 60 min/30 min cycle at a 50% depth of discharge and 10% overcharge. All plates were subjected to 100 cycles. The testing was carried out in flooded medium with two oversized counterelectrodes. The electrodes were cycled on a Tyco-built battery cycler with appropriate power supplies and recording equipment. The record parameters were: (a) capacity after formation, (b) charge and discharge potentials during cycling, (c) capacity after 100 cycles, (d) capacity limits between which the cycling occurred, and (e) physical changes (weight loss, shedding, etc.) The detailed experimental procedure was as follows:

1. Test plates were assembled in a cell with two overdesigned counter-electrodes in 30% KOH.

2. The plates were formed by 3 full cycles at the C/2 rate with 100% overcharge. The delivered capacity of the formed plate was then determined.

3. The formed plates were scrubbed to remove loosely-adherent surface material if necessary and then washed, dried, and weighed.

4. The cell was reassembled using 30% KOH.

5. The plate capacity was measured at the C/2 rate by a full discharge after charging with 100% overcharge.

6. The plates were cycled (60/30 min cycles, 50% depth of discharge, 10% overcharge), starting with the discharge portion of the cycle, from 80% state-of-charge for negative plates and 100% state-of-charge for positive plates. The cycling was carried out at room temperature for 100 cycles in a N_2 purged plastic box.

The plaque used in the manufacture of both the positive and negative plates, designated TY-19, contained the 25 mesh 0.005-in. nickel wire substrate as proposed in our design. Five plaques, 4 × 4 in., were impregnated in 2.0 M $Ni(NO_3)_2$, 0.3 M $NaNO_2$, 0.1 M $Co(NO_3)_2$, (105°C) at 0.5 A/in.^{2} for 85 min. The resulting mean theoretical capacity was 3.30 Ahr with a standard deviation of 0.086 (2.6% at 1σ level). Five additional plaque (4 × 4 in.) were passivated and then impregnated in 2.0 M $Cd(NO_3)_2$, 0.3 M $NaNO_2$, 105°C. at 0.5 A/in.^{2} for 37 min. The resulting mean theoretical capacity was 5.35 Ahr with a standard deviation of 0.109 (2.0% at the 1σ level). Fig. 17 illustrates the experimental setup. In Table XXII are listed plaque and capacity data for the electrodes used in this test. Figs. 18 and 19 show the IR corrected potential curves for typical charge and discharge cycles of positive and negative electrodes, respectively.

The positive electrodes were tested, starting from 100% state-of-charge on a discharge cycle to 50% depth of discharge and then charged with 10% overcharge. These electrodes typically cycled between 7 and 57% of their capacity, which suggests that the 10% overcharge was not sufficient to offset the charge inefficiency due to oxygen evolution at this rate and test temperature of 23°C. The data does indicate that the electrodes performed quite uniformly and predictably.

The negative electrodes were tested starting from 80% state-of-charge on a discharge cycle to 50% depth of discharge and then fully charged with 10% overcharge. These electrodes cycled typically between 17 and 67% of their total capacity. Again, the data indicates a high degree of uniformity.

Visual inspection of both positive and negative plates disclosed no apparent changes in the plates. A slight weight loss in the negative plates was noted (with subsequent decrease in capacity), although no such change occurred in the positive plates.
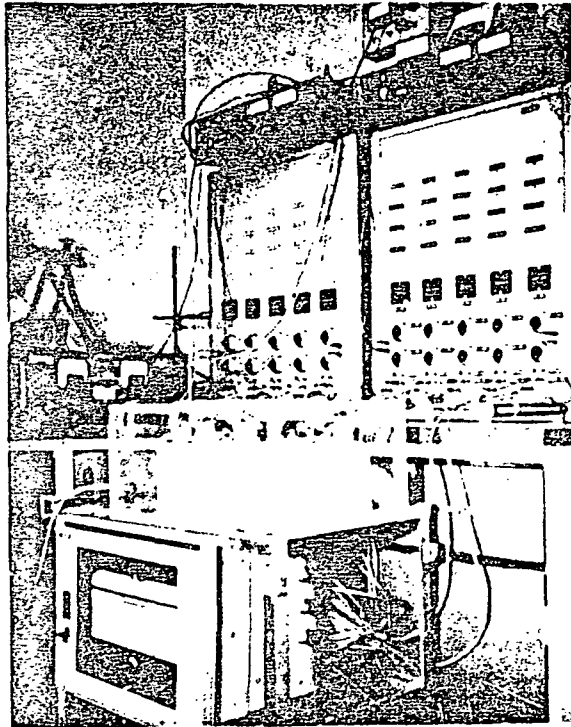
Fig. 17. Experimental setup used to test cell plates in simulated near-earth orbit cycling regime

Positive Electrode	Plaque Thickness (mils)	Plate Thickness (mils)	Plate Thickness After Formation (mils)	Theoretical Capacity	Revised Theoretical Capacity	After Formation, Delivered Capacity	Delivered Capacity 100 Cycles	Theoretical Capacity After 100 Cycles	Apparent Porosity	Powder Porosity
2	26.1	28.1	28.1	3.26	3.20	2.71	2.55	3.22	80.1	83.4
3	26.8	29.2	28.6	3.24	3.08	2.13	2.37	3.09	79.9	83.1
4	26.2	28.3	27.9	3.23	3.04	2.13	2.37	3.05	80.2	83.4
5	28.8	31.1	30.5	3.42	3.30	2.33	2.42	3.30	80.0	83.0
7	28.8	30.7	30.0	3.37	3.21	2.16	2.55	3.23	78.3	81.2
Negative Electrode										
1	26.2	28.4	26.7	5.29	4.41	3.15	3.03	4.12	80.0	83.3
8	26.4	29.3	27.1	5.51	4.45	3.28	2.96	4.21	80.0	83.2
11	26.6	28.3	26.8	5.28	4.32	3.15	2.84	4.05	80.3	83.6
14	25.9	29.0	26.4	5.42	4.50	3.21	3.05	4.20	79.9	83.2
15	25.8	27.9	26.2	5.25	4.45	3.10	3.05	4.12	79.8	83.2

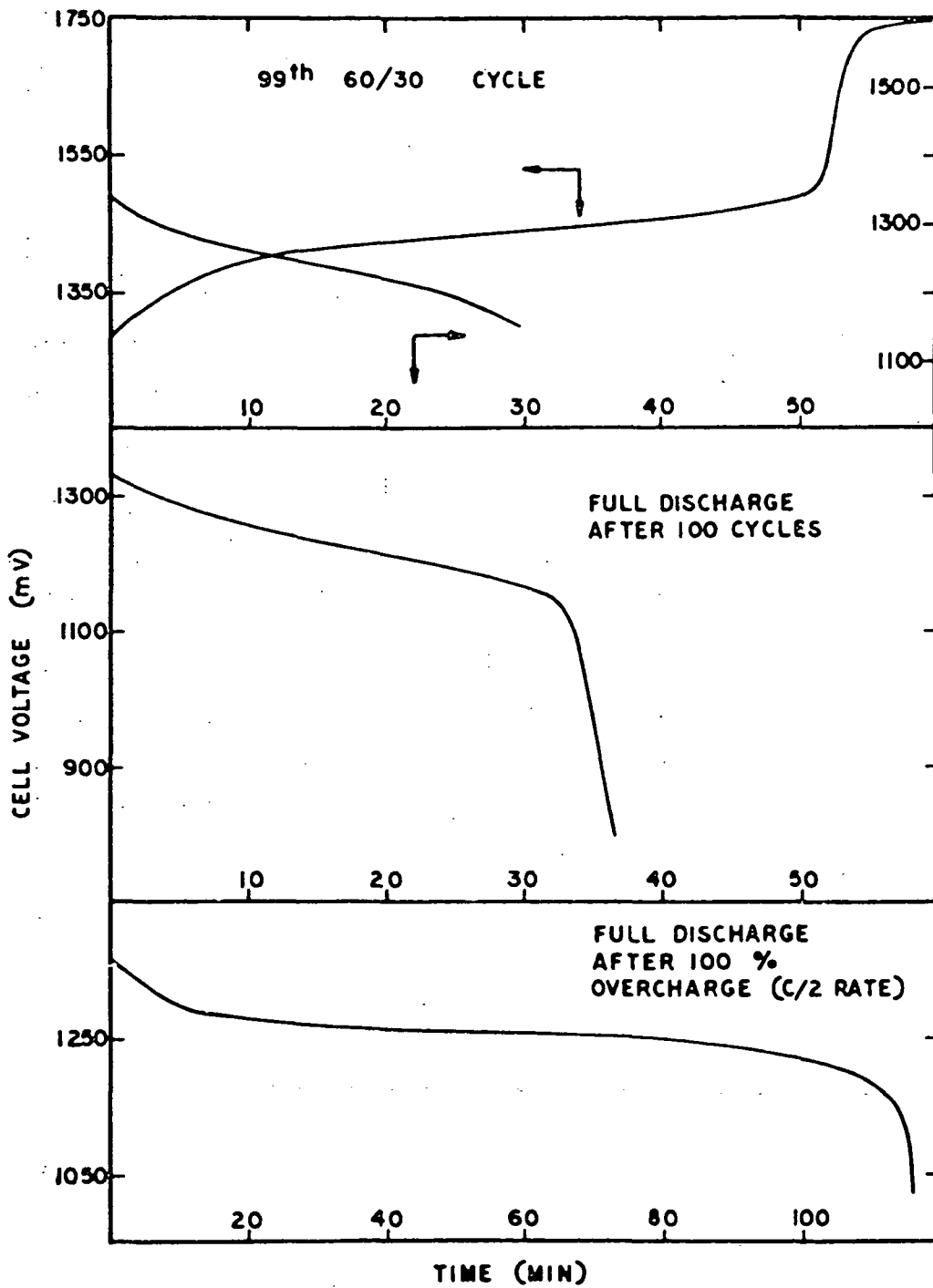Table XXII. 100 Cycle Test Electrode and Capacity Data

55

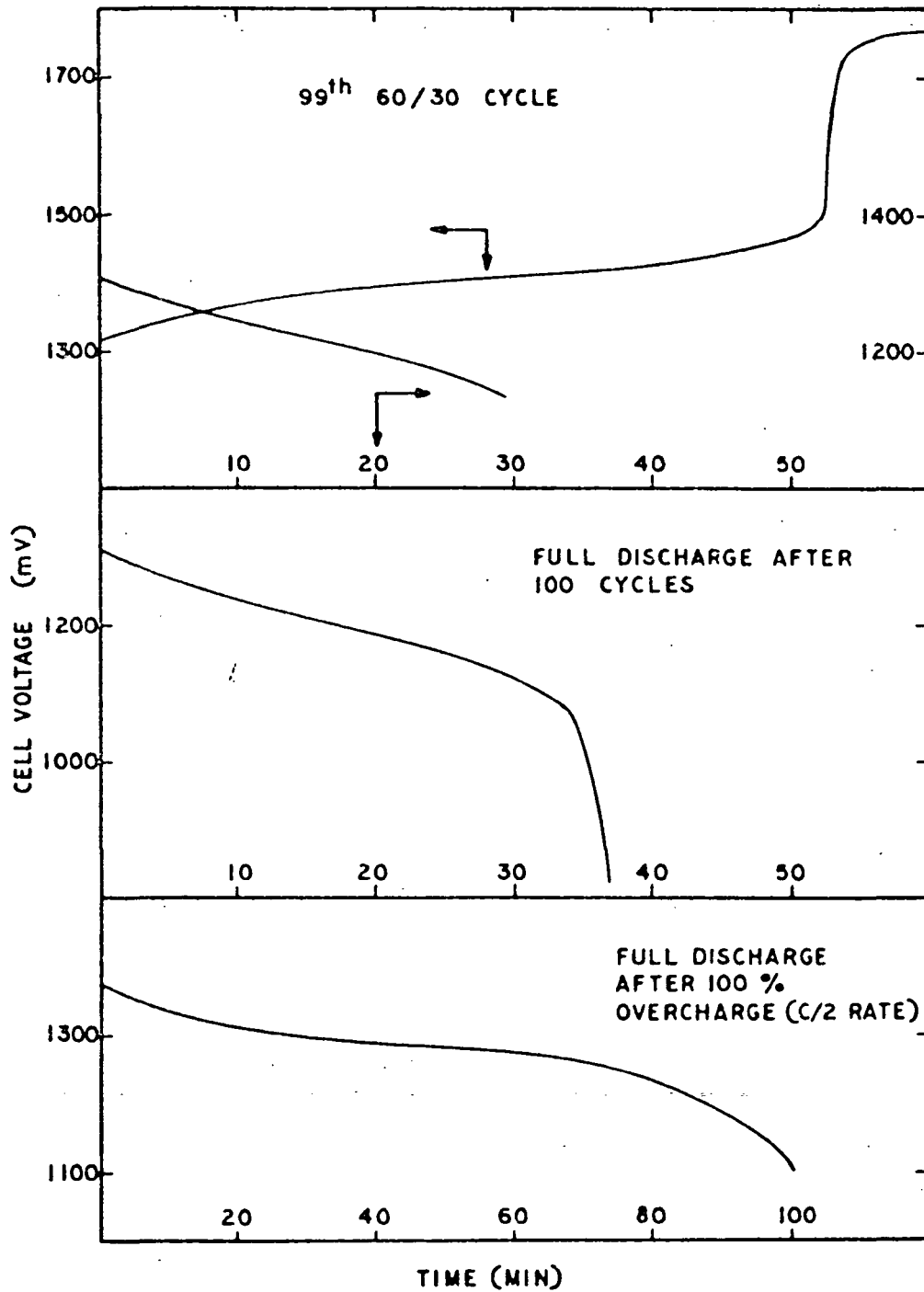Fig. 18. Typical positive electrode potential-time curves

Fig. 19. Typical negative electrode potential-time curves

Further analysis of the positive electrode capacity data generated during the simulated near earth orbit flooded testing pointed out that although the positive capacities were stable during the 100 cycles, a decrease in delivered capacity occurred after formation and prior to the start of the test. It was suspected that the plates may have been contaminated by carbonate ion. In order to resolve this, the plates were treated by a proprietary carbonate removal procedure and retested. This was necessary since nickel carbonates are not particularly soluble, and to analyze for total carbonate ion would necessitate destruction of the plate and subsequent gas analysis. After treatment the plates were retested in fresh 30% KOH and the plate efficiency was improved. Data are presented in Table XXIII. Improved handling techniques of plates in contact with CO_2 was established. It was also discovered that the ACS grade KOH used in making up the test solutions contained up to 1.0% K_2CO_3 (10,000 ppm). During the rest of the program, mercury cell grade ($< 0.03\%$ K_2CO_3) KOH was used for all test solutions.

Table XXIII   Effect of Carbonate Ion on Positive Plate Delivered Capacity

Plate Identity	Theoretical Capacity After Formation	Capacity After Formation	Capacity Prior to 100 Cycles	Capacity After 100 Cycles	Capacity After Carbonate Treatment	Final Efficiency (%)
TY-19-2	3.20	—	2.71	2.55	3.05	95
-3	3.08	3.45	2.13	2.37	2.95	96
-4	3.04	3.52	2.13	2.37	2.95	97
-5	3.30	3.72	2.33	2.42	3.00	91
-7	3.21	3.64	3.64	2.16	2.55	99

It was reported in the 6th Monthly Report of this contract that after formation of negative plates in 30% KOH, the delivered capacity was approximately 70% of the original theoretical capacity based on weight gain after impregnation. A portion of this reduced delivered capacity was due to the decrease in plate weight after formation. This means that in order to produce a negative electrode with the energy density specified in our design, higher loadings had to be achieved. In order to document our

58

ability to manufacture plates of this loading, a series of plaques was prepared for impregnation under conditions similar to those described in the Sixth Monthly Report of this contract with increased impregnation times proposed. The plaque selected for this work was from run TY-18, having a 20×20 mesh nickel wire substrate, nominal 30.5 mil thickness, and powder porosity of 82.5%. The plaques were lightly passivated prior to impregnation in a bath consisting of 2.0 M $Cd(NO_3)_2$ and 0.3 M $NaNO_2$, at its boiling point (105°C). The current density was 0.5 A/in.^{2}, and the impregnation times are listed in Table XXIV along with other pertinent data.

Comparing these data with data generated in a similar manner using TY-16 plaque, a striking dissimilarity in the weight gain versus impregnation time curves is noticed after approximately the 20-min impregnation time. This is clearly illustrated in Fig. 20, which compares weight gain versus impregnation time at 0.5 A/in.^{2} in identical impregnation solutions for both plaque types TY-16 and TY-18. Each of these plaque types was produced from identical compositions and similar manufacturing conditions, and therefore their physical characteristics appear similar as shown in Table XXV.

The apparent reason for the difference in impregnation behavior between the two plaque types seems to be associated with the fact that the TY-18 plaque had been passivated prior to impregnation whereas the TY-16 had not, since its data was generated prior to the introduction of the passivation procedure. This supposition is borne out in the fact that a sample of TY-18 plaque which had not been passivated and impregnated for 45 min showed a decreased weight gain compared to a passivated plaque. It has been previously pointed out that plaque which has been passivated shows negligible corrosion during impregnation and also is inhibited from forming large deposits of active material on the plaque surface, which, of course, drastically increases the final plate thickness. Previously reported negative plate thickness increases at lower current densities than presently used, and impregnation times of 25 min typically were less than 0.5 mil. With current densities of 0.5 A/in.^{2} and impregnation times of up to 45 min, there is a further increase in plate thickness, although this amounts to approximately 3 mils at 45 min impregnation time as opposed to a nonpassivated plaque increasing in thickness to over 11 mils during a 45 min impregnation.

Table XXIV. TY-18 Negative Plate Data

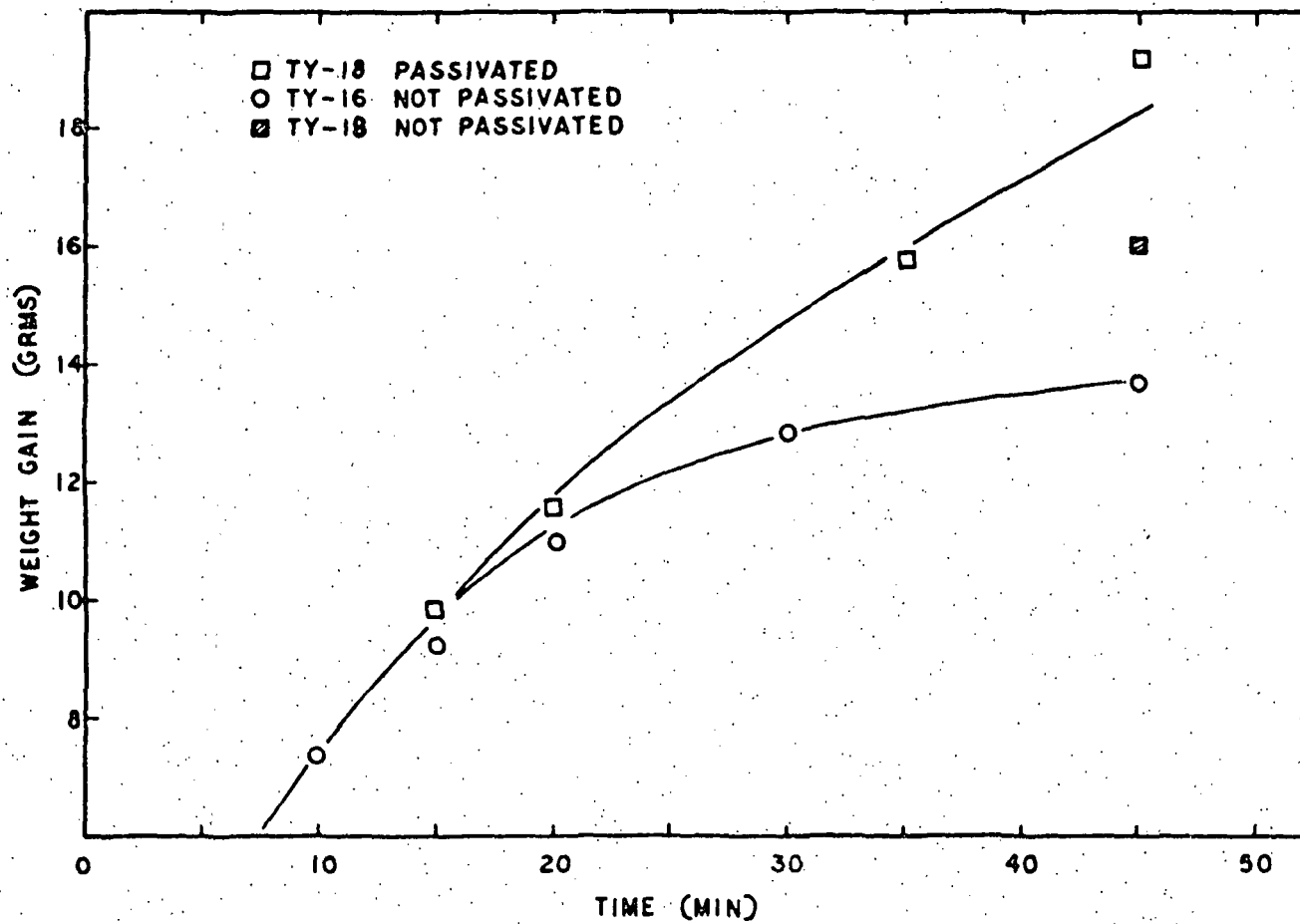| Plaque No.	Impregnation Time (min)	Plaque Thickness (mils)	Plate Thickness (mils)	Theoretical Capacity (Ahr)	Revised Theoretical Capacity (Ahr)	Delivered Capacity (Ahr)
21	20	30.8	31.2	4.27	-	-
22	20	31.2	31.2	4.23	-	-
23	20	31.3	31.2	4.42	-	-
24	20	31.0	31.0	4.32	-	-
38	35	30.7	31.2	6.02	5.0	3.93
42	35	30.4	31.4	5.82	5.0	4.03
40	45	29.6	33.4	7.07	6.19	4.83
43	45	29.7	33.1	7.01	6.06	4.63
89	5	30.7	30.7	0.90	-	-
90	10	30.5	30.6	1.71	-	-
91	15	30.3	30.4	3.59	-	-

60

Fig. 20. Impregnation characteristics of passivated and unpassivated plaque used in manufacture of negative plate

Table XXV. Physical Characteristics of TY-16 and TY-18 Plaque

Plaque	Sintered Thickness (mils)	Apparent Porosity (%)	Powder Porosity (%)	Resistivity (Ω-cm $\times 10^{-4}$)	Mechanical Strength (kg/cm²)
TY-16	29.0	78.3	82.6	6.1	88.2
TY-18	30.5	77.8	82.5	6.1	96.4

With this additional need for higher initial loadings due to the comparatively low efficiency of the negative electrode many possible alternatives were considered. The goal here has been the manufacture of a negative plate which has a delivered capacity of 9 Ahr/in.^{3} Under the optimum negative impregnation conditions developed earlier in this contract, it appeared that delivered loadings of 8.5 Ahr/in.^{3} were readily achievable. An increase in the coulombic input to obtain the slightly higher loading results in an amount of an unwanted surface buildup of active material. To totally appreciate this problem, a variety of factors must be considered, for which we shall refer to Fig. 21. Fig. 21 relates various loading levels of negative plate with the plaque thickness and its associated weight which would contain these levels. Moving up or down any of the lines of the graph does not change the amount of total capacity delivered but merely shows its possible distribution for 83% porous nickel plaque. It appears that the use of 83% porous plaque having a thickness of 28 mils will not allow us to achieve the correct negative plate loading, and therefore the proper negative to positive capacity ratio. An increase in either or both the plaque porosity and thickness seemed necessary to achieve our goals. Since our design has specified a positive to negative capacity ratio of 1:1.4, any decrease in negative capacity would obviously alter this ratio downwards. The intersection of the achieved 8.5 Ahr/in.^{3} loading and the plate thickness of 28 mils describes this ratio.

A first possibility was to increase the design plaque thickness which would increase the void volume available to active material deposition. It can be seen from the graph that at the 1.4 to 1 negative to positive ratio, an increase in plaque thickness from 28 mils to 31.2 mils would allow the necessary capacity to be delivered at a loading level of 8.9 Ahr/in.^{3} instead of 9.0 Ahr/in.^{3} Obviously as can be seen from Fig. 21 this involves an increase in the plaque weight from 0.694 g/in.^{2} to 0.77 g/in.^{2} Such an increase in negative plaque weight has the effect of increasing the total cell weight by less than 3%, which still allows our cell design to exhibit a substantial increase in energy density over other cells.
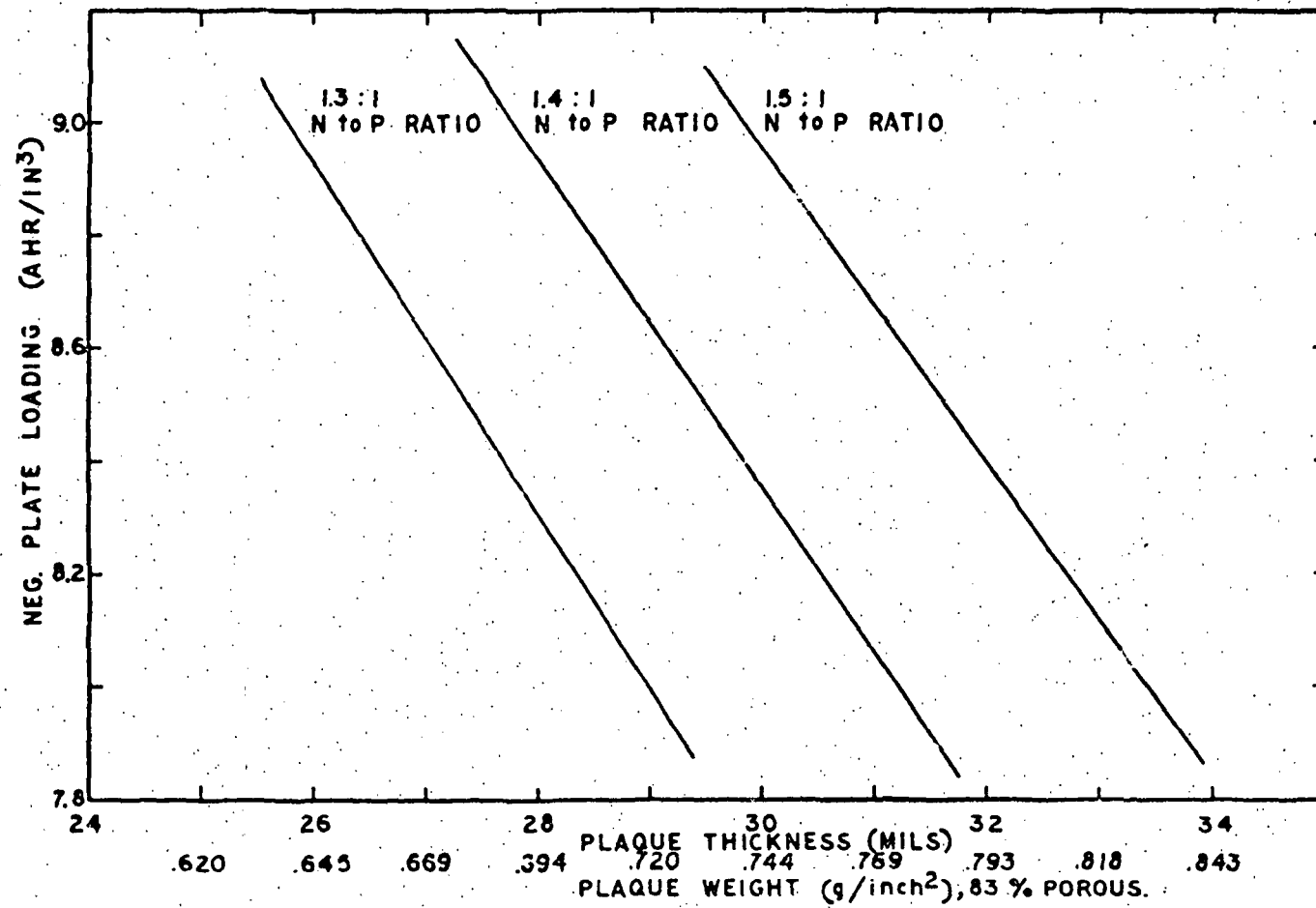
Fig. 21. Various negative plate loadings related to plaque thickness and weight at different negative-positive capacity ratios

63

Another alternative is demonstrated by considering the effects of increasing the plaque porosity from 83% to 85%. By calculation it is seen that a 28-mil. 85% porous plaque has a weight of only 0.612 g/in.^{2} as opposed to that of an 83% porous plaque which weighs 0.694 g/in.^{2} For an 85% porous plaque to weigh 0.694 g/in.^{2}. it would have to be approximately 31.7 mils thick. According to our graph. at the 1.4:1 ratio such a plaque would need to be loaded to less than 8.0 Ahr/in.^{3} to deliver the necessary capacity, and yet it would still meet the weight requirement proposed in the design.

Of the possible solutions indicated above. the most reasonable one appeared to be that of increasing both the plaque porosity together with increasing the plaque thickness to allow for the acceptance of the higher loadings. Towards this end, a number of plaques were manufactured with an increased sinter porosity and plaque thickness and impregnated as outlined in the Eighth Monthly Report. Results are presented below in Table XXVI

In the far right column of the table is the plate capacity expressed as Ahr/in.^{2} of plate. The value necessary to maintain the 1.4 to 1 negative to positive capacity ratio is 0.25 Ahr/in.^{2} It can be seen from these data that when using plaque having the above characteristics, negative plate of the proper loading may be manufactured without penalizing the original designs' weight savings. It was therefore proposed to specify that negative plate be manufactured from plaque having a sinter porosity of 83 ± 1% and a thickness of 0.030 in. ± 0.0005 in.

Table XXVL Tyco Negative Plate Characteristics

Plate Identity	Plaque Thickness (mills)	Sinter Porosity (%)	Plate Thickness (mils)	Thickness After Formation (mils)	Theoretical Capacity (Ahr)	Delivered Capacity (Ahr)	Capacity (Ahr/in^2)
TY-28-4	29.8	84.3	30.4	29.7	5.50	3.90	0.244
-6	28.7	84.1	29.6	28.9	5.38	3.90	0.244
-7	27.8	84.3	29.2	29.0	5.54	3.90	0.244
-8	28.5	84.0	32.2	30.6	5.55	3.90	0.244
TY-27-39	29.4	83.9	30.1	29.8	6.50	4.17	0.261
-42	30.1	84.1	31.1	30.9	6.47	4.02	0.251
-43	30.0	84.0	31.1	30.6	6.12	4.13	0.258

65

V. CELL TESTING

A. 4-Ahr Cells

Five 4-Ahr, hermetically sealed NiCd cells were assembled and tested in the starved condition using a simulated inclined synchronous orbit regime. Each of the five cells was manufactured using a batch process due to the quantities involved and assembled in a previously designed nickel-plated steel cell can. The plates, both positive and negative, were produced using slurry-coated Ni sintered plaque of a nominal thickness of 29.0 mils and a sinter porosity of 83%. Table XXVII shows the various plaque characteristics.

The impregnation of both positive and negative plates was carried out in solutions and under conditions described and documented previously.

As can be seen from Table XXVII, the uniformity of the plaque material is quite acceptable.

Table XXVIII shows the capacity data for these plaques after batch impregnation and formation. The variability of the plate material is a result of this type of batch processing, yet this material is acceptable for the purpose of testing our cell design. Typical reproducibility of plate capacity is exemplified by data shown in Table XXVIX. These plates were manufactured by the continuous impregnation process, and it is obvious from the data that this produces a highly uniform product. Once the plates were impregnated and formed, they were cut to the proper size and grouped to achieve the desired negative-to-positive capacity ratio of 1.4:1.0.

Table XXX lists the groupings of the electrodes used in each of the five cells along with the flooded value of capacity and the capacity ratio. It was determined that in the worst case, the variation in plate capacity was 2.5% at the $1\text{-}\sigma$ level for negative plates in a particular cell and 2.2% at the $1\text{-}\sigma$ level for positive plates. The plates were stacked up in alternate layers. When the stacking was completed, each

Table XXVII. Plaque Characteristics

Negative Electrodes

Plaque No.	Thickness (mils)	Apparent Porosity (%)	Powder Porosity (%)
1	0.028475	79.11	82.07
2	0.0287	79.45	84.0
3	0.0286	79.72	84.30
4	0.0298	79.89	84.29
6	0.0287	79.59	84.14
7	0.0278	79.57	84.29
8	0.0285	79.40	83.98
17	0.02842	78.93	82.86
30	0.02865	78.87	83.40
31	0.0297	78.92	83.28
32	0.02975	79.02	83.38
33	0.02998	79.44	83.79
34	0.02981	79.25	83.61
35	0.03004	79.18	83.50
36	0.02978	79.13	83.49

Positive Electrodes

Plaque No.	Thickness (mils)	Apparent Porosity (%)	Powder Porosity (%)
10	0.02856	78.76	83.30
11	0.0288	--	--
12	0.0283	78.09	82.63
13	0.0287	--	--
14	0.0287	78.28	82.71
15	0.0286	--	--
16	0.0285	73.85	82.78
18	0.030	79.20	83.53
19	0.0294	78.85	83.25
20	0.0296	78.99	83.37
21	0.0292	78.87	83.31
22	0.0298	79.26	83.63
23	0.0298	79.05	83.40
24	0.0297	79.16	83.55
25	0.0298	78.99	83.34
26	0.0302	79.61	83.93
27	0.0292	78.51	83.01
28	0.0302	79.26	83.56
29	0.0295	78.69	83.07

Table XXVIII Capacity Data for 4-Ahr Cell Electrodes

Positive Electrodes

Plate No.	Revised Theoretical Capacity (Ahr)	Delivered Capacity (Ahr)	% Efficiency
18	2.677	3.44	128
19	2.94	3.68	125
20	3.13	4.08	130
21	3.106	4.01	129
22	3.152	4.08	129
23	3.046	3.99	131
24	2.953	3.66	125
25	3.215	4.01	125
26	3.025	3.96	131
27	2.973	3.55	119
28	3.139	4.07	130
29	3.025	3.82	126

Negative Electrodes

Plate No.	Revised Theoretical Capacity (Ahr)	Delivered Capacity (Ahr)	% Efficiency
30	4.33	3.33	76.91
31	5.172	3.93	75.98
32	4.72	3.53	74.78
33	4.39	3.23	73.57
34	4.726	3.63	76.80
35	4.65	3.60	77.42
36	4.632	3.23	69.73
17	4.931	3.40	68.95
2	4.313	3.53	81.8
3	4.543	3.60	79.2
4	4.743	3.90	82.2
6	4.678	3.90	83.3
7	4.783	3.90	81.6
8	4.776	3.90	81.8

Table XXVIX. Typical Positive Plate Manufactured by a Continuous Process

Plate No.	Theoretical Capacity (Ahr)	Delivered Capacity (Ahr)
206	1.975	2.21
208	1.950	2.16
211	1.967	2.13
212	1.846	2.08
213	1.834	2.16
216	1.852	2.16
217	1.853	2.13
218	1.894	2.16
231	1.872	2.08
232	1.884	2.08
233	1.911	2.21
234	1.853	2.19
236	1.846	2.13
238	1.893	2.21
240	1.822	2.11
241	1.879	2.16
244	1.830	2.21
245	1.910	2.13
246	1.919	2.19
247	1.863	2.16
Mean	1.88	2.15
Standard deviation	0.045	0.044

Table XXX. 4-Ahr Cells

Cell Identity	Positive* Plates	Positive Capacity (Ahr)	Negative* Plates	Negative Capacity (Ahr)	Capacity Ratio Positive to Negative
TY-227-4-1	(4) No. 18 (4) No. 27	5.03	(4) No. 17 (4) No. 30 (2) No. 36	7.08	1:1.41
TY-227-4-2	(4) No. 20 (4) No. 19	5.29	(4) No. 2 (4) No. 32 (2) No. 3	7.53	1:1.42
TY-227-4-3	(4) No. 29 (4) No. 26	5.59	(4) No. (4) No. (2) No.	7.68	1:1.37
TY-227-4-4	(4) No. 23 (4) No. 21	5.75	(4) No. 4 (4) No. 6 (2) No. 7	8.25	1:1.43
TY-227-4-5	(4) No. 25 (4) No. 28	5.81	(4) No. 8 (4) No. 31 (2) No. 7	8.29	1:1.43

* ( ) indicates the number of electrodes cut from that particular plate.

stack was wrapped temporarily with Teflon tape and aligned with the cell cover assembly, which included the cell terminals. The electrode leads from the stacks were then spot welded to the appropriate terminal. The stacks were compressed and slid into the cell can with an outside layer of separator material surrounding the stack. Each cell cover was then heliarc welded to the can with appropriate heat sinks protecting the terminals and cell body. The cells were leak tested and then filled with 30% KOH. The electrolyte fill level was determined prior to this time by saturating an identical stack-up of electrodes and separator material in a bottomless cell can with electrolyte and allowing the stack to drain. The amount of electrolyte retained was considered the 100% fill level. The actual cells were filled to 80% of this value. Each cell was then precharged to 10% of its negative capacity by first fully charging

the cell while sealed and then evacuating the cell while continuing the charge for the appropriate amount of time. The cell was permanently sealed while still under vacuum by pinching the fill tube and welding it shut. These cells were then placed on an automatic cycler to be tested under a simulated inclined synchronous orbit regime. This regime consists of a 23-hr charge at the C/10 rate (0.40 A) followed by a 1-hr discharge to 60% depth (2.4 A). A typical early cycle is shown in Fig. 22.

This testing continued for over 100 days (> 100 cycles). The final (complete) discharge curves of each of the five cells is shown in Figs. 23 through 27. These final discharges were obtained by allowing the cells to discharge beyond the 1 hour at 2.4 Amp mark and indicate the total capacity of the cells after test.

It can be seen from the preceding data that according to the potential time curves these cells appear to behave in a reproducible and predictable manner. It can be also seen from the data in Table XXXI that there is a loss in delivered capacity during cycling. First of all, the efficiency, Pc/Tc suggests that the fill level of the cells is slightly low, the target value for the fill level was 80%. Upon visual examination of cells, it was discovered that three of them, numbers 1, 2 and 4 had small pinholes in the weld area of the can. This was probably due to the use of the nickel plated steel cans which tend to oxidize during welding, forming pockets of dross in the weld area. Upon subsequent leak testing the weld appears to be tight but upon contact with the electrolyte these products corrode and form gas leakage paths. This in turn, with time, causes the loss of water and the apparent loss of cell capacity due to drying. It is suggested that Cells No. 3 and 5 also "dried out" somewhat but by a slower leakage path - past the O-ring seals at the cell terminals. This was evidenced by minute quantities of corrosion products around the bases of all terminals.

Thus, these tests suggest that with a proper hermetic seal the cells could properly operate under this type of test regime.

B. 12-Ahr Cells

Based on the design considerations discussed in Section II-D, the results discussed under Section IV-C, and the data generated from the testing of 4-Ahr size cells, five 12-Ahr rated cells were designed and built. The electrode design specifications are listed in Table XXXII. The cell case was constructed of 15 mil thick Type 304L stainless steel with all welded seams. The terminal closures were effected by the use of modified Ziegler, i.e., crimped polymeric, seals. The cell component drawings and attribute sheets are found in Appendix I. To further enhance
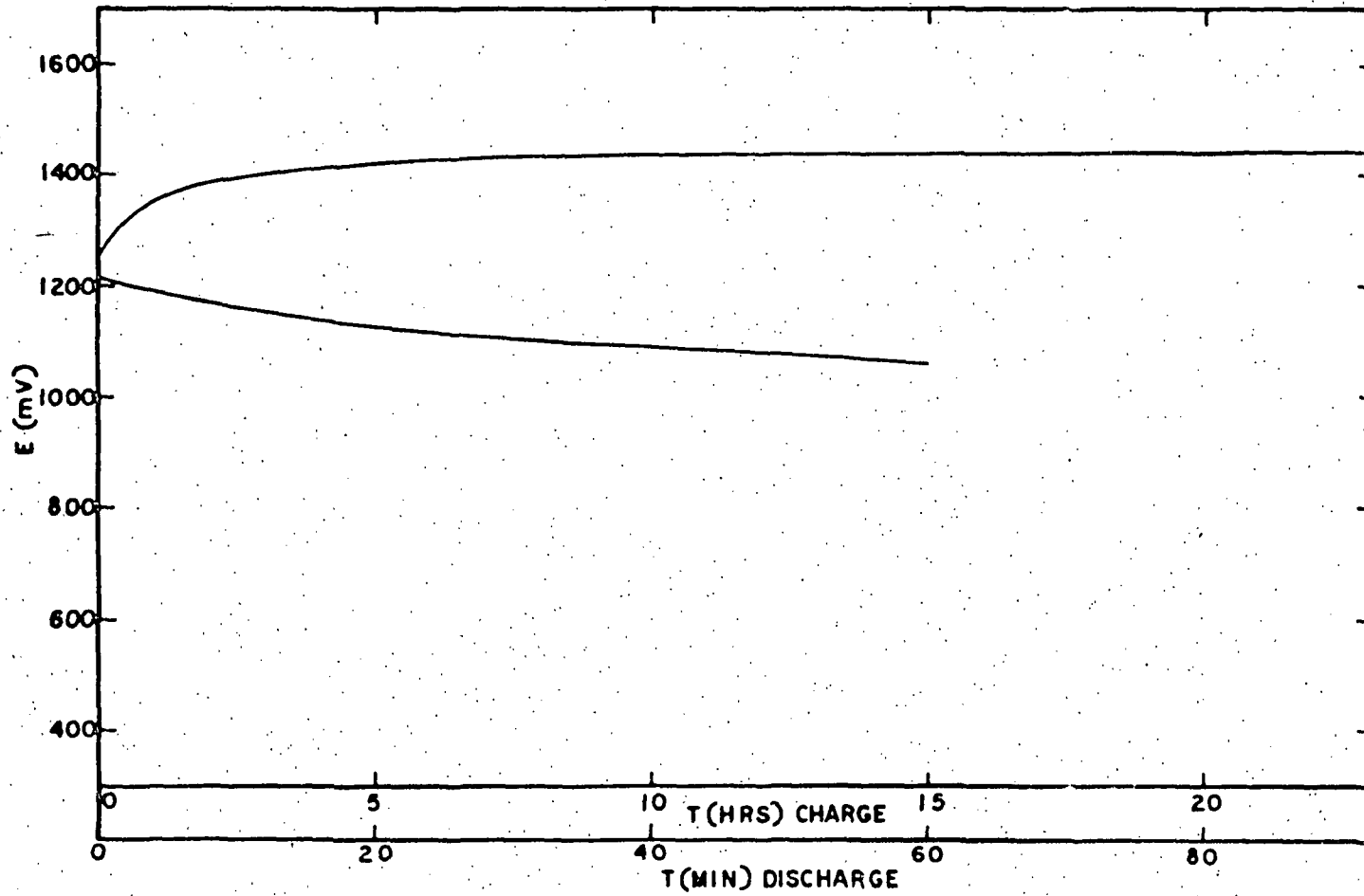
72

Fig. 22. Typical charge-discharge curves for 4-Ahr cell under simulated inclined synchronous orbit
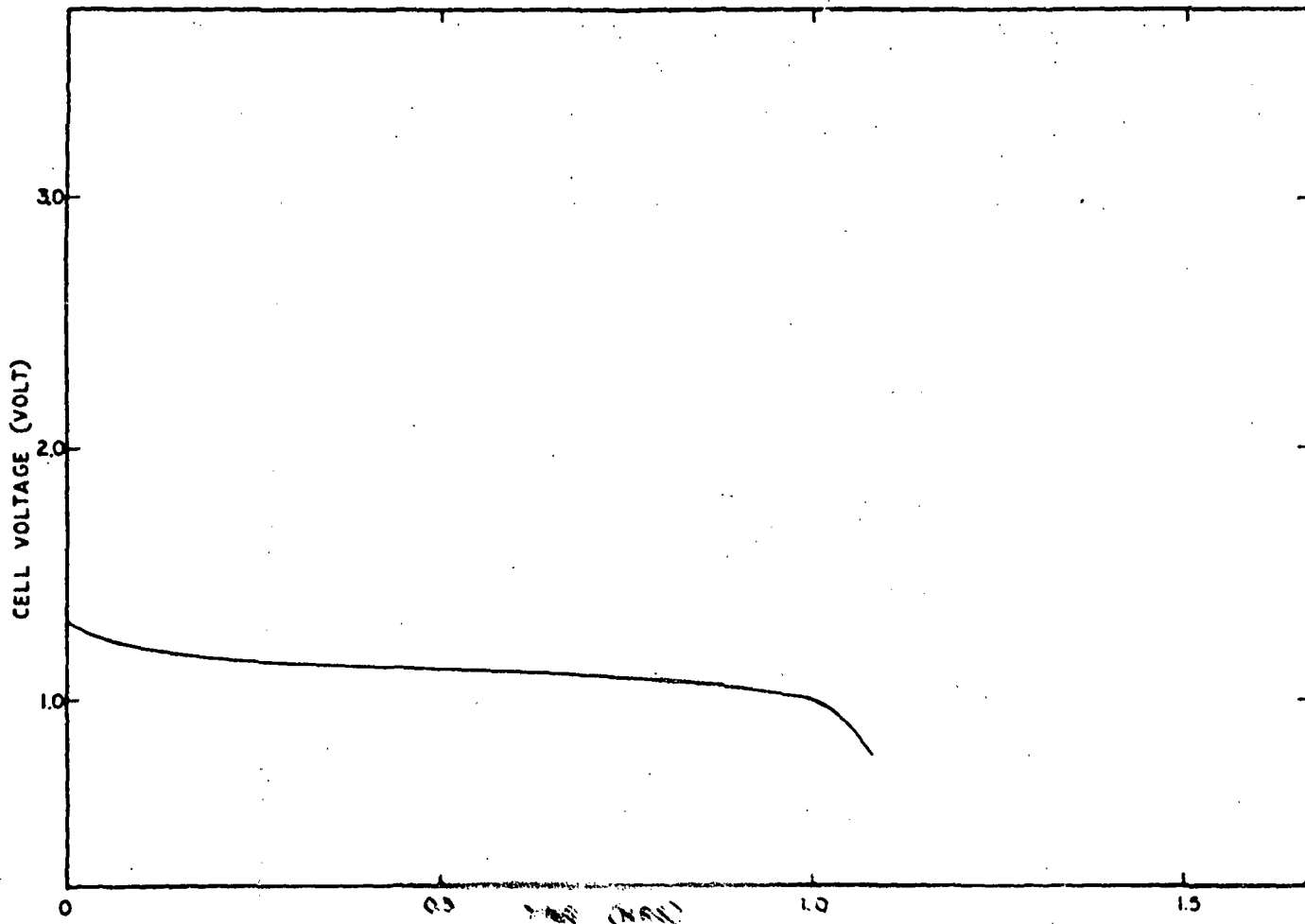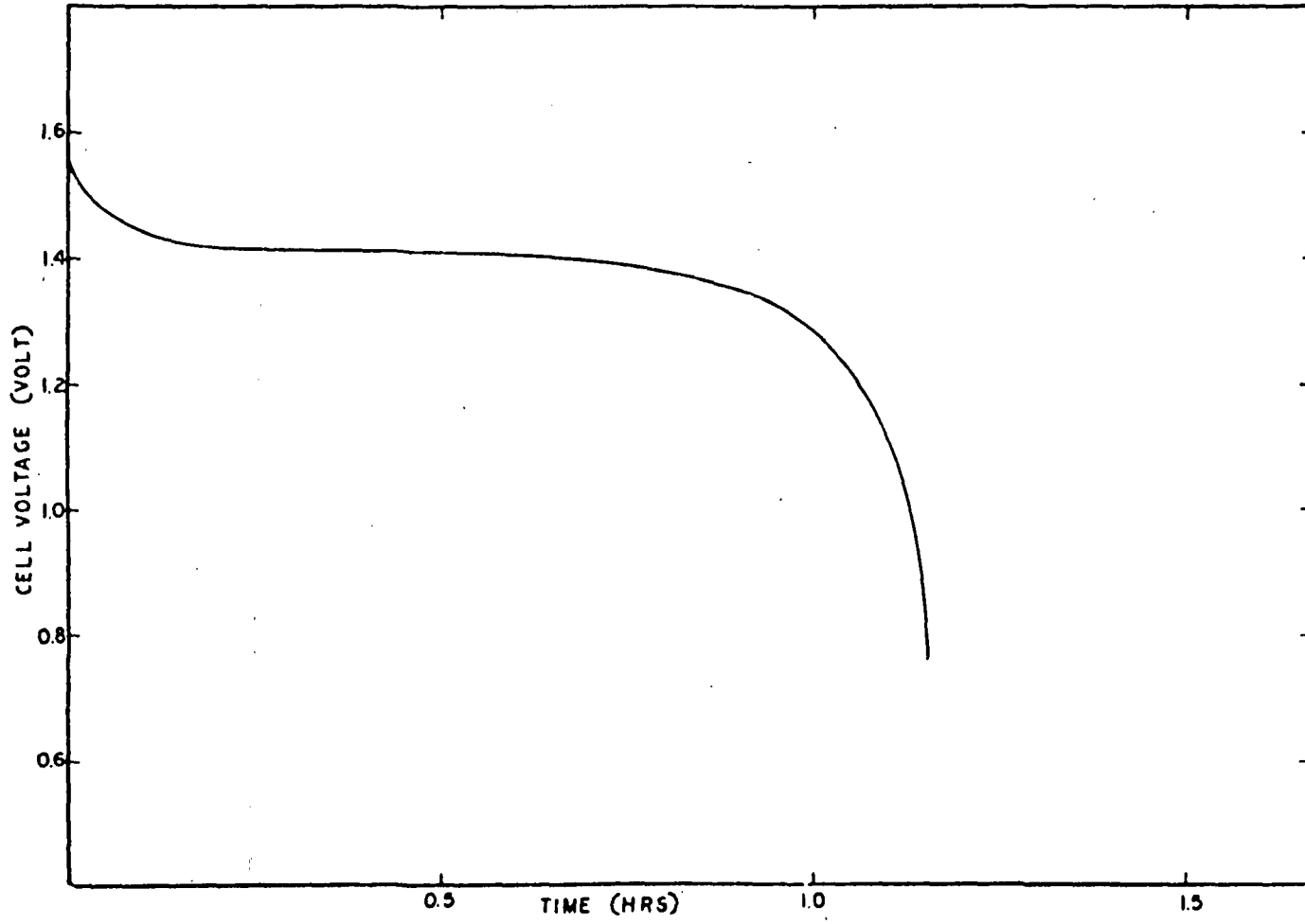cycling regime

Fig. 88 Cell No 1 final discharge > 100 cycles
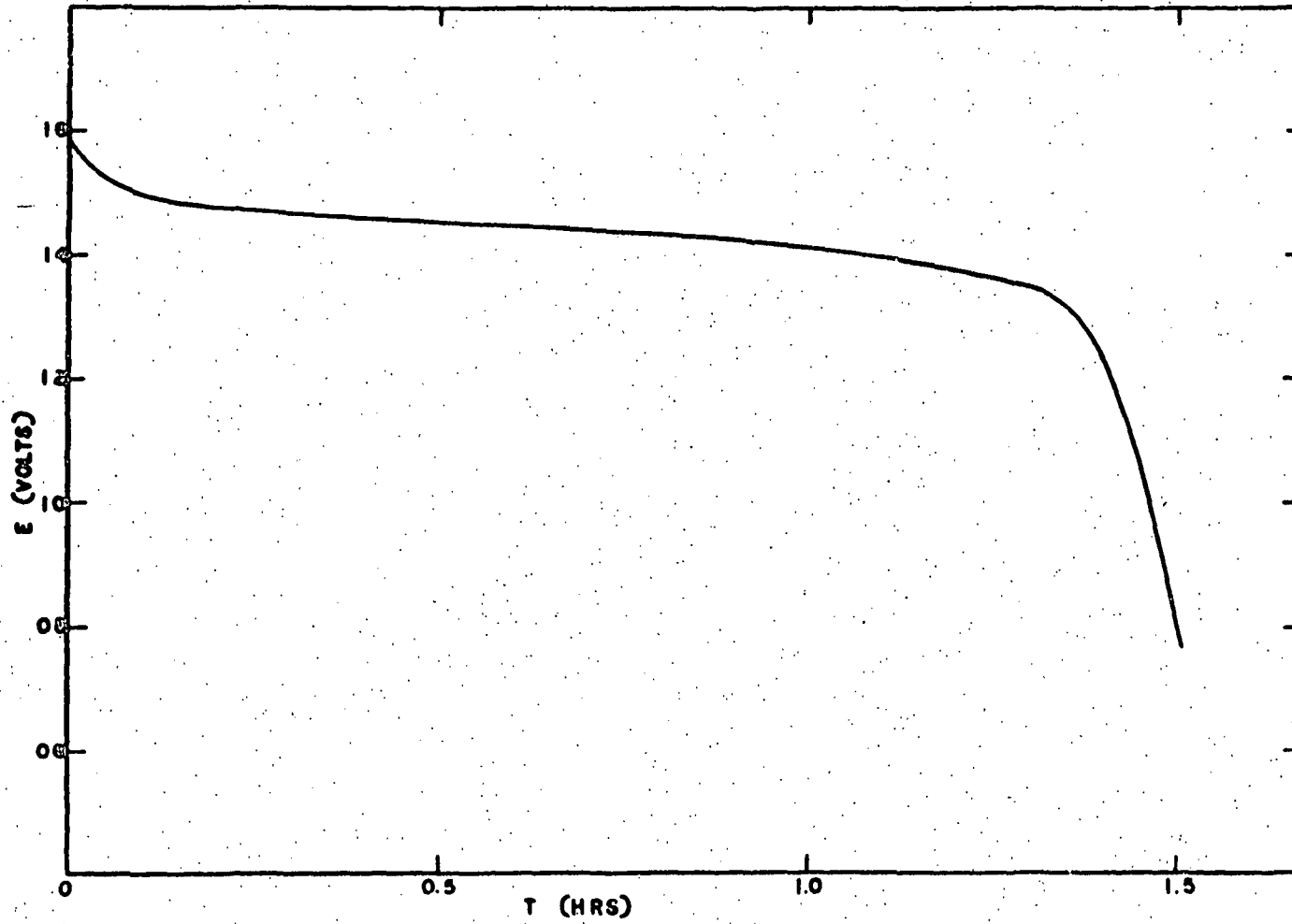
74

Fig. 24. Cell No. 2 final discharge > 100 cycles

Fig. 25. Cell No. 3 final discharge > 100 cycles

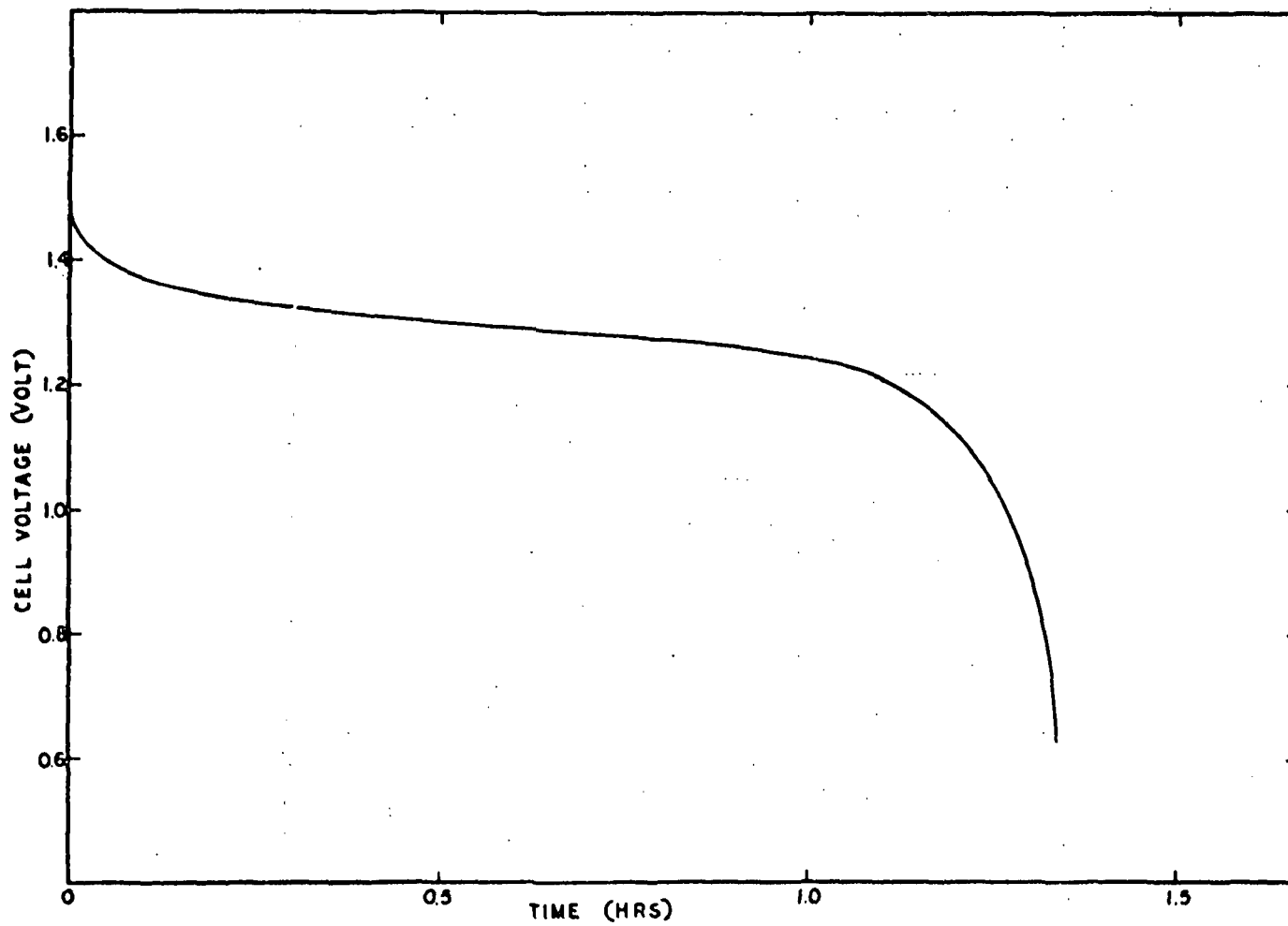Fig. 26. Cell No. 4 final discharge > 100 cycles
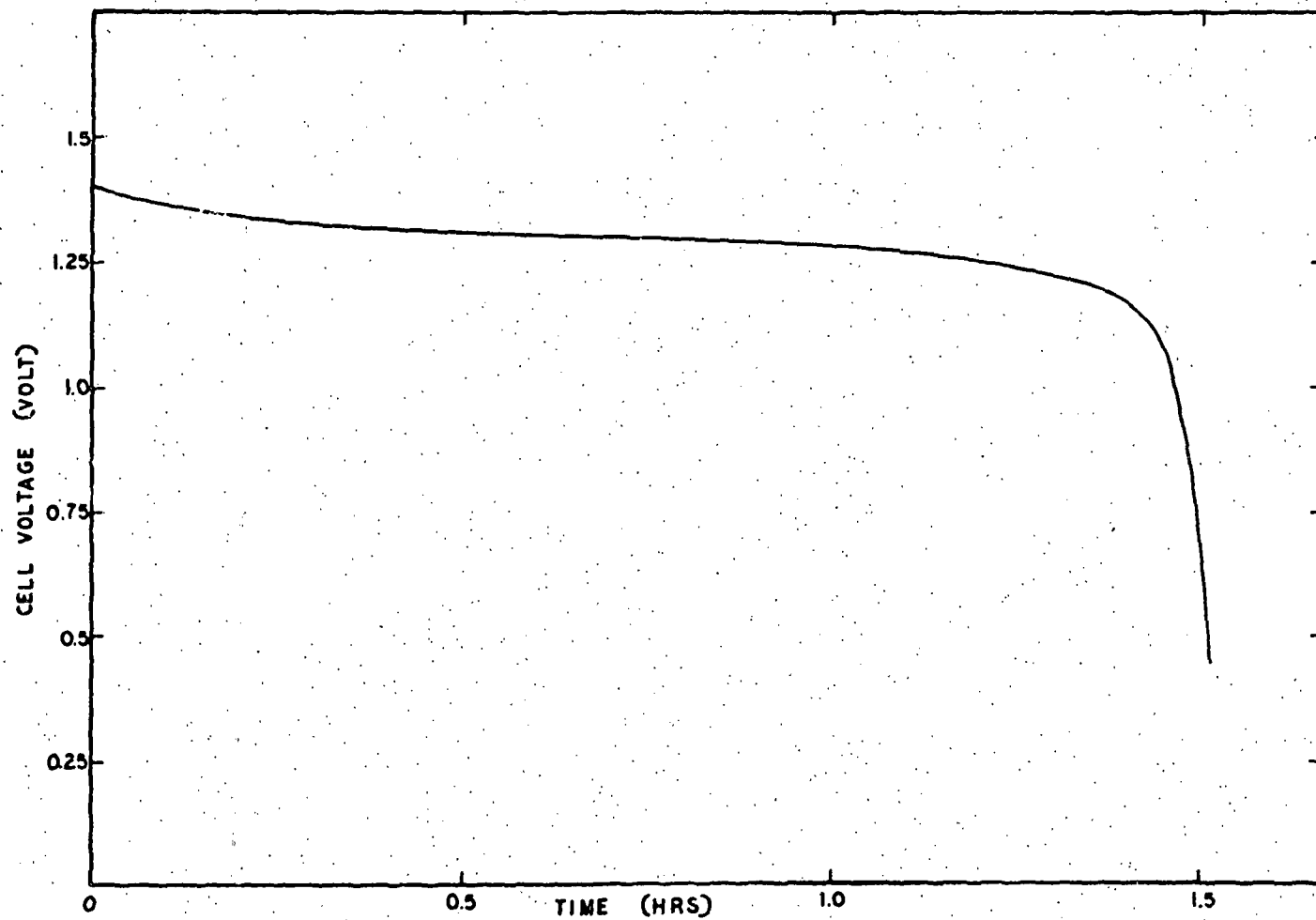
Fig. 27. Cell No. 5 final discharge > 100 cycles

Table XXXL 4-Ahr Cell Capacity Data

Cell No. 227-4-	T_c Theoretical (flooded) Capacity (Ahr)	P_c Capacity After Precharge (Ahr)	F_c Capacity After 100 Cycles (Ahr)	Efficiency P_c/T_c (%)	Efficiency F_c/P_c (%)
1	5.03	3.93	2.64	78.0	67.2
2	5.29	3.93	2.80	74.5	71.2
3	5.59	4.27	3.64	76.5	85.2
4	5.75	4.14	3.12	72.0	75.4
5	5.81	4.14	3.64	71.0	87.9

Table XXXII. Electrode Design Specifications for 12-Ahr Cell

Positive Plate

1. Number of plates - 10
2. Plate size - 3.25 × 2.8 in. (± 0.01)
3. Substrate - 0.005 in. nickel wire screen at 25 mesh
4. Plaque type - sintered nickel powder
5. Plaque porosity - 83% ± 1%
6. Plaque thickness - 0.028 in. ± 0.0005 in.
7. Plaque weight variation - ± 0.05 g/in.^{2}
8. Plate capacity - 0.200 Ahr/in.^{2}, flooded
9. Plate capacity variability - max 2% at 1 σ level
10. Carbonate level max 1%

Negative Plate

1. Number of plates - 11
2. Plate size - 3.25 ± 2.8 in. (± 0.01)
3. Substrate - 0.005 in. nickel wire screen at 25 mesh
4. Plaque type - sintered nickel powder
5. Plaque porosity - 83% ± 1%
6. Plaque thickness - 0.030 in. ± 0.0005 in.
7. Plaque weight variation - ± 0.05 g/in.^{2}
8. Plate capacity - 0.257 Ahr/in.^{2}, flooded
9. Plate capacity variability - max 3% at 1 σ level
10. Carbonate level max 1%

the validity of the Tyco design a direct comparison of our projected cell was made with the actual characteristics of a commercial 12-Ahr aerospace quality cell.

The commercial cell was tested for its electrochemical capacity by charging at ~C/3 rate (4A) with 50% overcharge and then discharged at 4 A. This test was repeated and the average delivered capacity of the cell was found to be 15.8 Ahr, much higher than was expected. Since this capacity exceeded the design value for the Tyco 12-Ahr cell and since both cells are similar in weight and physical size, it was felt that a direct analysis of its cell components would be beneficial in pin-pointing differences in the two cells. The following table compares some of the more pertinent physical and electrochemical characteristics of the two cells.

Component	Commercial Cell	Tyco Cell
1. Cell Can		
Dimensions (outside)	$0.875 \times 2.98 \times 4.00$ in.	$0.800 \times 2.95 \times 4.00$ in.
Material thickness	0.018 in.	0.015 in.
Weight	85 g	70 g
2. Positive Plate		
Single plate weight	13.04 g	12.9 g
Total plate weight	143.4 g	129.3 g
Unit weight	1.67 g/in.^{2}	1.41 g/in.^{2}
Active material weight	~ 57 g (calculated)	52.5 g
Number	11	10
Size	2.8×2.75 in.	3.25×2.8 in.
Area	7.8 in.^{2} (86 total)	9.1 in.^{2} (91 total)
Thickness	32 mil	28 mil (30 final)
Screen type	4 mil perforated	5 mil, 25 mesh screen
Starved capacity (ave)	1.44 Ahr/plate (0.184 Ahr/in.^{2})	1.47 Ahr/plate (0.162 Ahr/in.^{2})
Cell capacity (starved)	15.8 Ahr (tested)	14.7 Ahr
3. Negative Plate		
Single plate	12.74 g	15.6 g
Total plate weight	152.9 g	172.2 g
Plate unit weight	~1.63 g/in.^{2}	1.72 g/in.^{2}
Active material weight	0.811 g in.^{2}	0.827 g/in.^{2}
Number	12	11
Size	2.8×2.75 in.	2.8×3.25 in.
Area	7.8 in.^{2} (93.5 total)	9.1 in.^{2} (100.1 total)
Thickness	29 mil	30 mil
Screen type	4 mil perforated	5 mil, 25 mesh screen
Flooded capacity (tested, delivered)	1.53 Ahr/plate (0.195 Ahr/in.^{2})	2.34 Ahr/plate (0.256 Ahr/in.^{2})

Component	Commercial Cell	Tyco Cell
3. Negative Plate (continued)		
Total negative capacity (flooded)	18.4 Ahr (tested)	25.76 Ahr
Total theoretical capacity*	27.8 Ahr	30.3 Ahr
Total starved negative capacity**	18.8 Ahr	20.6 Ahr

*Based on chemical analysis for active material in plates.
**Assuming 80% fill level and 85% efficiency of the negative electrodes, based on theoretical.

It appears that from the actual measured values of negative plate capacity, the Tyco design provides for a larger ratio of negative to positive capacity.

It appears that a much lower negative-to-positive capacity ratio is being utilized in the commercial cell with a resultant weight decrease. A more definite weight comparison is shown in the table below.

Component	Commercial	% Total	Tyco Cell	% Total
Separator	8.2 g	1.7	10.0 g	2.1
Third electrode	1.7 g	<1.0	1.7 g	< 1.0
Plastic shield	3.2 g	< 1.0	-	-
Top assembly, terminals, etc.	25.0 g	5.2	33.0 g	6.9
Positive electrodes	143.4 g	29.8	129.3 g	27.0
Negative electrodes	152.9 g	31.8	172.2 g	36.0
Can	85.0 g	17.7	70.0 g	14.6
Electrolyte	62.0 g	12.9	62.0 g	13.0
Total weight	481.0 g	100%	478.0 g	100%

If the positive-to-negative capacity ratios are calculated, it is found that in the starved mode the Tyco cell is designed to deliver a ratio of 1:1.4. On the other hand, the commercial cell positive-to-negative ratio appears to be 1:1.19. On a theoretical basis, the commercial cell does have a P to N ratio of 1:1.4 but the design apparently neglects the inefficiency of the negative electrode. Also, it appears from a comparison of the weight of the commercial cells' negative active material and the resultant <u>flooded</u> capacity that the efficiency of the negative plates is actually lower

than the 85% level consistently found in Tyco negative plates. All this, of course, results in a further lowering of the available negative capacity, a decreased P to N ratio and a shorter cell life expectancy.

Formulation difficulties involving the slurry coated plaque material necessitated the acceptance of plaque material to be used for negative plate manufacture with a lower than desired porosity. Porosity values for plaque Lot Nos. 7366 and 7369 used in the manufacture of the cells were 80.1 ± 0.5%. The other physical characteristics of the plaque runs suggested their suitability for use in the assembly of the five prototype cells. The reasoning behind this decision was that the goal was to prove the validity of the design at the sacrifice of the long life characteristics of the cell. Impregnation of positive plaque Lot No. 7367A proceeded under conditions discussed previously. The results, after formation, showed that the flooded capacity values were 1.80 ± 0.09 Ahr.

Similarly, negative plaque was impregnated under previously described conditions with the result that negative plates were produced with an average flooded capacity of 2.18 Ahr. Variance at the 1 σ level was approximately 4.6%, 50% beyond the desired 3.0% at the 1 σ level.

Both positive and negative plates were formed in 30% KOH (mercury cell grade) using oversize active counterelectrodes. The plates were charged and discharged three cycles at the C/2 rate, the final cycle used to determine the actual capacities noted above.

After rinsing, drying, and inspection the plates were grouped in cell units of 10 positives and 11 negatives. Polypropylene separators were fitted around the negative plates and the plates were then welded to the electrode combs using the appropriate heat sinks to protect the active areas of the electrodes. The combs were then welded to the terminal feet which were previously positioned in the top assembly. With the third (reference) electrode positioned against the side of the electrode stack, the entire unit was slid into the stainless steel cell can. After checking for shorts the top assembly was welded to the can, using the appropriate heat-sinks to protect the active elements inside the can. The modified Ziegler seals were then crimped and each cell was then tested for leaks using a helium leak detector. Cells were then filled with 40 cc of 30% mercury cell grade KOH. This amount of electrolyte had been experimentally determined previously, using an additional cell core, to be the 80% fill level. Each cell was then weighed and immediately fitted with a stainless steel pressure gauge and closure valve system used to adjust the negative precharge to approximately 15% of the available negative capacity. The cell weights are shown in Table XXXIII.

83

Table XXXIII. Cell Weight Data

Cell No.	Electrolyte Weight (g)	Cell Weight, Filled (g)	Cell Weight With Gauge, etc. (g)	Wt, Positive Electrodes (g)	Wt, Negative Electrodes (g)
227-12-2	52	504.9	799.5	144.5	174.8
227-12-4	52	503.9	799.6	148.0	176.5
227-12-5	52	495.4	792.7	139.7	175.0
227-12-6	52	495.9	792.0	143.0	173.4
227-12-7	52	501.2	795.4	140.7	179.0

The precharge of the cells was initiated with a C/10 (1.2 A) charge for 16 hr. During this entire time cell voltage and pressure was monitored visually and recorded. At the end of this time the closure valves were opened and the cell evacuated to wa*_r vapor pressure while the charging current was increased to 2.5 A. This was continued for one hour after which the charging was discontinued and the cells sealed via the valve. The cells were then discharged at the C/6 (2.0 A) rate to a cell voltage cut-off of 1.0 V. Since the capacities appeared to be low, 5 cc of electrolyte was added and the cells re-evacuated. This was done with the assumption that the cells were too sta.ved. The cells were then again charged for 16 hr at 1.2 A and discharged at 2.0 A. Pertinent data is shown in Table XXXIV.

The evident difficulties experienced during this final testing of the prototype cells were due to an unfortunate combination of circumstances. First, the cells were restrained using thin aluminum plates which buckled considerably under the initial cell pressures. Then, due to the increase in electrolyte level and possibly a maladjustment in the charge, the second charge cycle generated even higher cell pressures further deforming the cell cases. Once the cases were deformed the electrodes could physically separate from one another in the stack. This of course, resulted in the even lower capacity due to lack of electrolyte in contact with the plates and inefficient charge acceptance. The excessive pressures were probably encouraged by the fact that lower than optimum porosity negative plaque was used in the plate manufacturing. It is well known that low porosity, highly loaded negative plates operate inefficiently for oxygen recombination. No further attempt was made

Table XXXIV. 12-Ahr Cell Data

Cell No.	First Charge Voltage (max)	Max Cell Pressure (psig)	Cell Capacity (Ahr)	Second Charge Voltage (max)	Max Cell Pressure	Cell Capacity (Ahr)
2	1.439	51	12.6	1.452	100+	9.7
4	1.424	62	12.0	1.427	32	11.1
5	1.433	56	11.3	1.426	95	9.3
6	1.429	60	13.1	1.450	100+	10.1
7	1.439	75	12.0	1.437	100+	9.7

to test these cells and due to the inability to procure additional cell cases no other cells were assembled.

In the best case it appears that we were able to produce a 12-Ahr rated cell delivering over 13 Ahr with an energy density of approximately 15 watt hours per pound.

VL CONCLUSIONS

The parameters involving the development of a highly reliable, aerospace quality NiCd cell with an improved energy density have been investigated and detailed. Weight reduction of plaque substrate and plaque sinter was shown to have a significant effect on the theoretical energy density of this system. Light weight screen substrate and plaque having an improved porous structure were employed in the manufacture of electrode materials for this contract.

It was again found that the high temperature electrochemical impregnation method was critically dependent on the physical characteristics of the porous nickel plaque. Uniformity of materials was controlled to produce high porosity plaque for the manufacture of plate with the best balance of high loadings and most efficient operation and utilization. Some difficulties in producing plaque in large quantities with the desired characteristics were attributed to changes in properties of the wet slurry upon scale-up from the experimental quantities employed to establish the plaque-plate relationships. The difficulty manifested itself in a plaque with a somewhat lower than desired sinter porosity.

The manufacture of positive plate was carried out after the successful determination of the necessary impregnation parameters. The effect of nickel in concentration, nitrite ion concentration, and current density were optimized to produce highly loaded positive plate with excellent utilization of the active materials within the porous structure.

The manufacture of negative plate was pursued in a similar manner. Plaque corrosion during impregnation was minimized by light oxidation of the surface. Difficulties were experienced in manufacturing the thicker plaque with the desired sinter porosity. The high loadings specified for the negative plate. in conjunction with the decreased porosity of the plaque led to less than desirable plate operation.

i.e., lower active material utilization. In addition, accumulation of nitrate ion in the bath during continuous impregnation led to deposition of active materials on the plate surface, not uniformly distributed within the plaque structure. Such problems resulted in the less than desired plate capacity variance of 4.6% at the 1σ level.

It appears that work in the future should consider problems associated with the continuous impregnation of negative plates. An obvious approach would be to discard the impregnation solution frequently. The disadvantages here are that such action interferes with the economics of the system and the flow of material of a major manufacturing operation. A more reasonable approach would be to study further the interaction of plaque with respect to the continuous impregnation of negative plate. The continuous electrochemical impregnation of positive plate seems to present less severe difficulties and is not nearly as sensitive to high bath nitrate concentrations.

In addition, the changing properties of large quantities of nickel powder slurry should be studied to determine the effects of time, temperature, mixing, etc. on the final sintered plaque.

VII. REFERENCES

1. "Heat Sterilizable and Impact Resistant Ni-Cd Battery Development," Final Report (January, 1970), Contract No. 951972 Mod 14.

2. M. H. Gottlieb and T. H. Willis, "Operating Characteristics of Sealed Nickel-Cadmium Batteries at Low Temperatures," J. Electrochem. Tech. $\underline{4}$. 515 (1966).

3. "Development of Uniform and Predictable Battery Materials for Nickel-Cadmium Aerospace Cells," Final Report (8 May 1968 - 31 Jan. 1972) Contract No. NAS5-11561.

4. "Development of Uniform and Predictable Battery Materials for Nickel-Cadmium Aerospace Cells," Interim Annual Report (8 August 1968 - 7 July 1969), Contract No. NAS5-11561.

5. "Development of Uniform and Predictable Battery Materials for Nickel-Cadmium Aerospace Cells," Interim Annual Report (8 November 1970 - 8 May 1971), Contract No. NAS5-11561.

6. Dean Maurer, private communication.

APPENDIX I

12-AH CELL COMPONENT ATTRIBUTE SHEETS AND
ASSOCIATED DRAWINGS

I-1

Attribute Sheet

Date:

Part No.:   T-12010
Part Name: Comb
Vendor:
Lot No.:
Lot Size: Sample Size:

Dimensions	Pieces O.K.	Pieces not within tolerance
A. 0.110		
B. 0.650		
C. 0.020 +0.002 − 0.000		
D. 0.800		
E. 1.00		
F. 0.037 +0.000 − 0.001		

Tolerances:

2 place ± 0.01
3 place ± 0.005
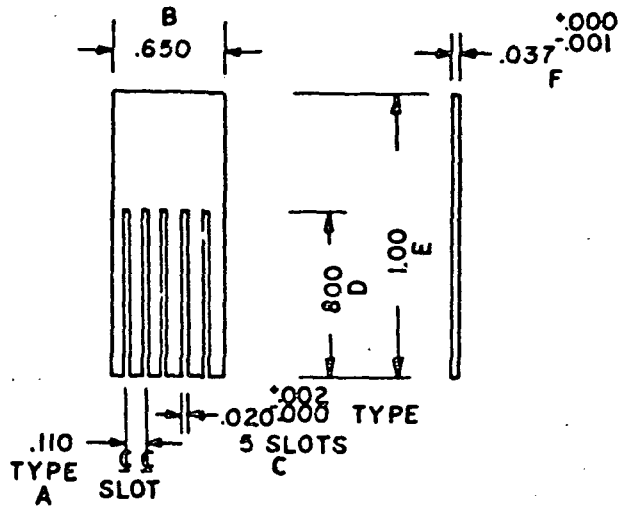
Inspected by:

I-2

Fig. 1-1. Comb-material Ni 200, Part No. T-12010

Attribute Sheet

Date:

Part No.:   T-12017
Part Name: Terminal
Vendor:
Lot No.:
Lot Size: Sample Size:

Dimensions	Pieces O.K.	Pieces not within tolerance
A. 0.250		
B. 0.125		
C. 0.125		
D. 0.040		
E. 0.150		
F. 0.500		
G. 0.800		

Tolerances:
   2 place ± 0.01
   3 place ± 0.005   Inspected by:
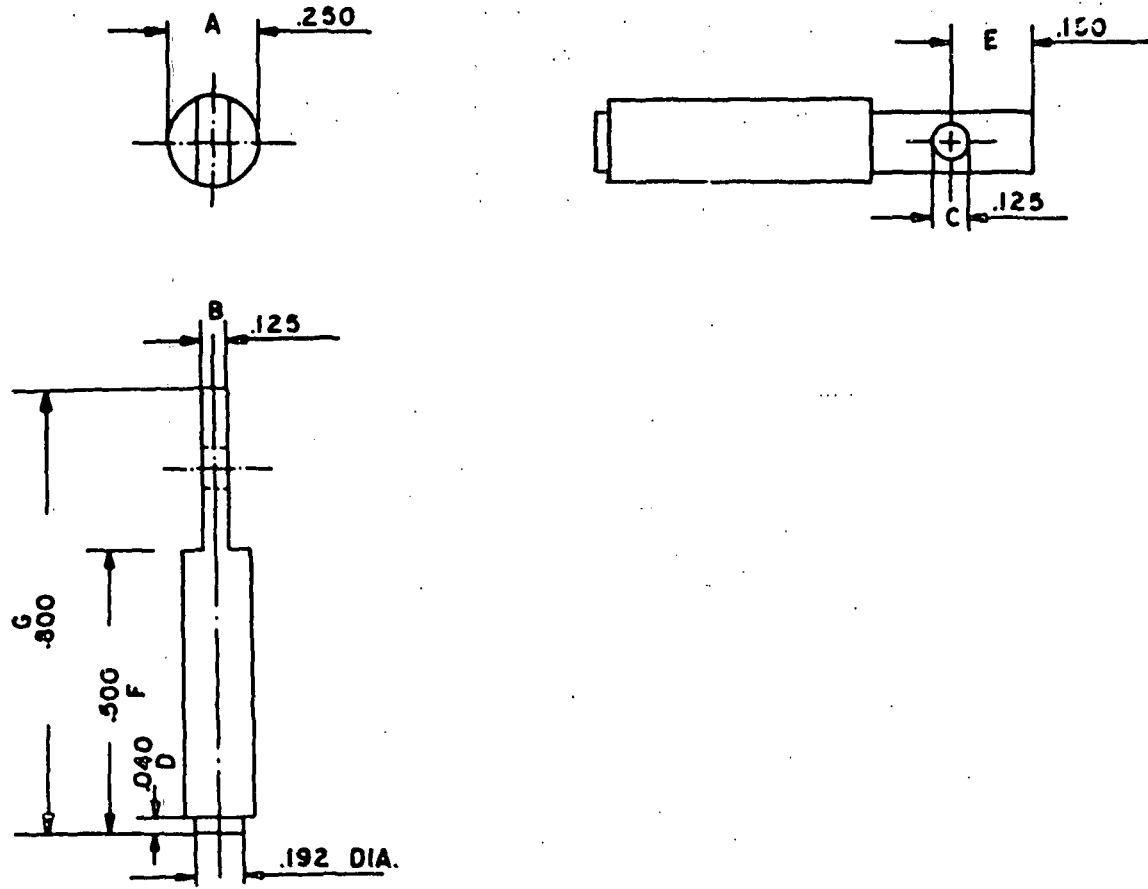
Fig. I-2. Terminal-material NI 200, Part No. T-12017

Attribute Sheet

Date:

Part No.:   T-12018
Part Name: Terminal Connector
Vendor:
Lot No.:
Lot Size: Sample Size:

Dimensions	Pieces O.K.	Pieces not within tolerance
A. 0.750		
B. 0.192		
C. 0.325		
D. 0.450		
E. 0.150		
F. 0.045		
G. 0.300		
H. 0.650		

Tolerances:

  .2 place ± 0.01
  3 place ± 0.005   Inspected by:
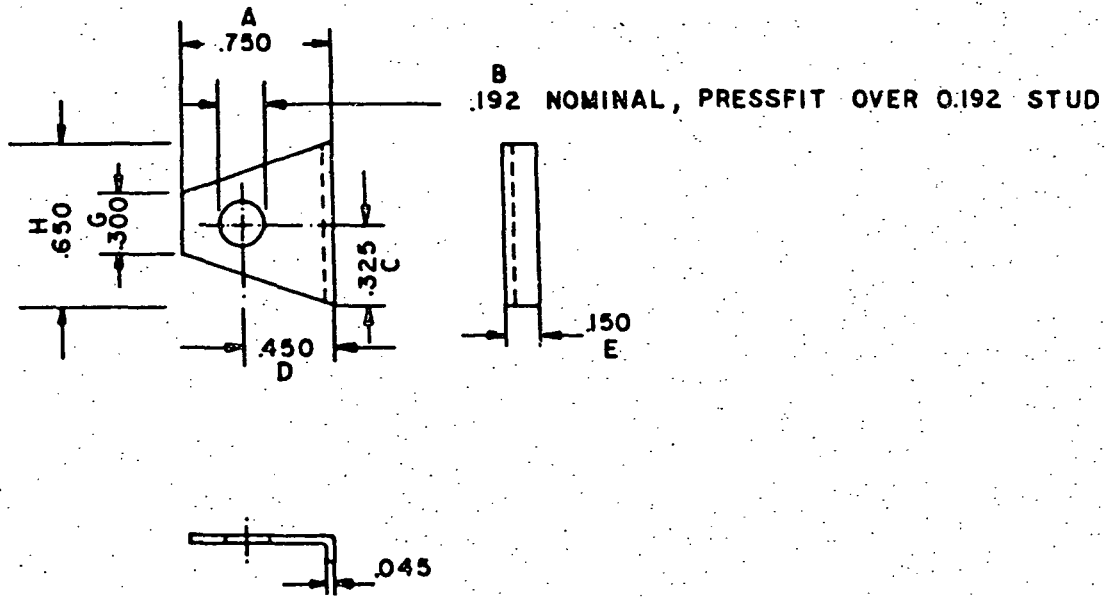
Fig. I-3. Terminal connector material Ni 200, Part No. T-12018

Attribute Sheet

Date:

Part No.:   T-12012
Part Name: Plaque Tab
Vendor:
Lot No.:
Lot Size: Sample Size:

Dimensions	Pieces O.K.	Pieces not within tolerance
A. 3.00		
B. 0.075		
C. 0.094		
D. 0.060		
E. 0.125		
F. 0.125		
G. 0.50		
H. 0.005		

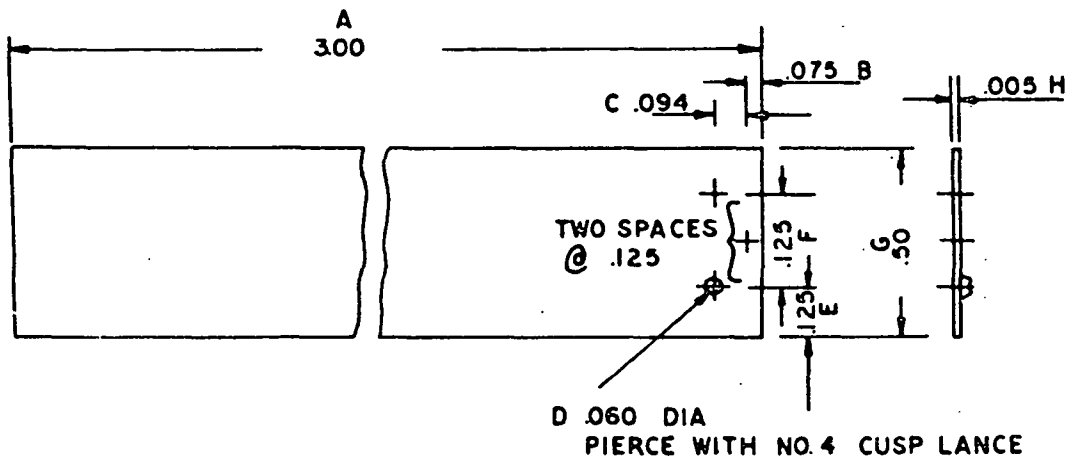Tolerances:
   2 place ± 0.01
   3 place ± 0.005

Inspected by:

Fig. I-4. Plaque tab material Ni 200, Part No. T-12012

Attribute Sheet

Date:

Part No.: T-12014
Part Name: Barrel Seal
Vendor:
Lot No.:
Lot Size: Sample Size:

Dimensions	Pieces O.K.	Pieces not within tolerance
A. 0.480		
B. 0.062		
C. 0.062		
D. 0.426		
E. 0.076		
F. 0.032		
G. 0.467 +0.000 −0.001		
H. 0.480		
L. 0.500		
J. 0.375		

Tolerances:
   2 place ± 0.00
   3 place ± 0.005

Inspected by:
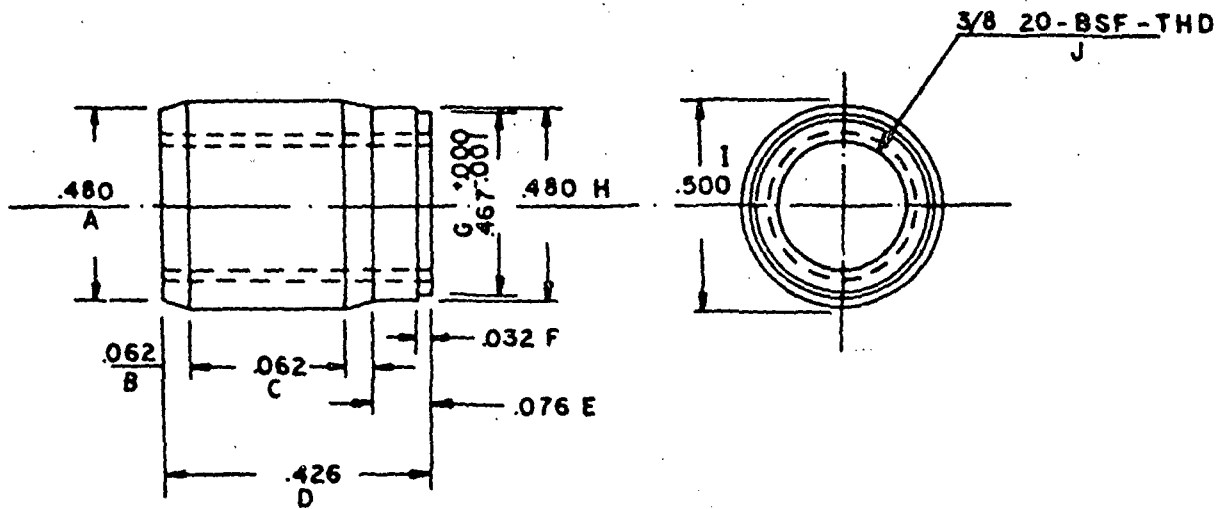
Fig. I-5. Seal barrel material 304L SS, Part No. T-12014

Attribute Sheet

Date:

Part No.:   T-12015
Part Name: Seal Barrel Insert
Vendor:
Lot No.:
Lot Size: Sample Size:

Dimensions	Pieces O.K.	Pieces not within tolerance
A. 0.750		
B. 0.250		
C. 0.375		
D. 1/16		
E. 1/16		

Tolerances:

    2 place ± 0.01
    3 place ± 0.005   Inspected by:

E 1/16 SCREW DRIVER SLOT

D 1/16

(DEBURR DIE RUNOUT)

250 ±002

0.75
A

SECTION AA

3/8 - 20 BSF THD
C
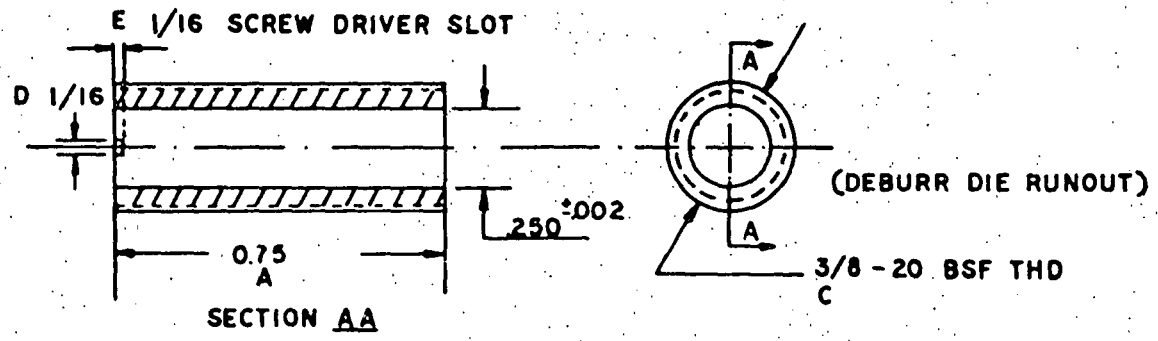
Fig. I-6. Seal barrel insert material - polypropylene, Part No. T-12015

Attribute Sheet

Date:

Part No.:   T-12016
Part Name: Tube, Fill
Vendor:
Lot No.:
Lot Size: Sample Size:

Dimensions	Pieces O.K.	Pieces not within tolerance
A. 0.060		
B. 1.50		
C. 0.030		
D. 0.106 +0.001 - 0.000		
E. 0.125		

Tolerances:

2 place ± __

3 place ± 0.005   Inspected by:
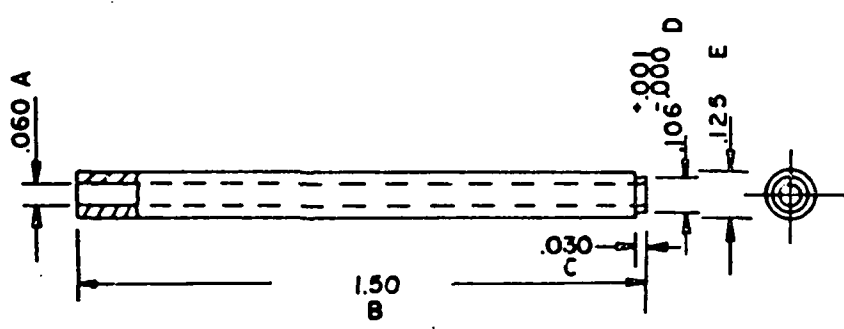
I-14

Fig. I-7. Fill tube material 304L SS, Part No. T-12016

Attribute Sheet

Date:

Part No.:   T-12100
Part Name: Can Assembly
Vendor:
Lot No.:
Lot Size: Sample Size:

Dimensions	Pieces O.K.	Pieces not within tolerance
A. 0.500		
B. 4.00		
C. 0.015		
D. 2.95		

Tolerances:
    2 place ± 0.00
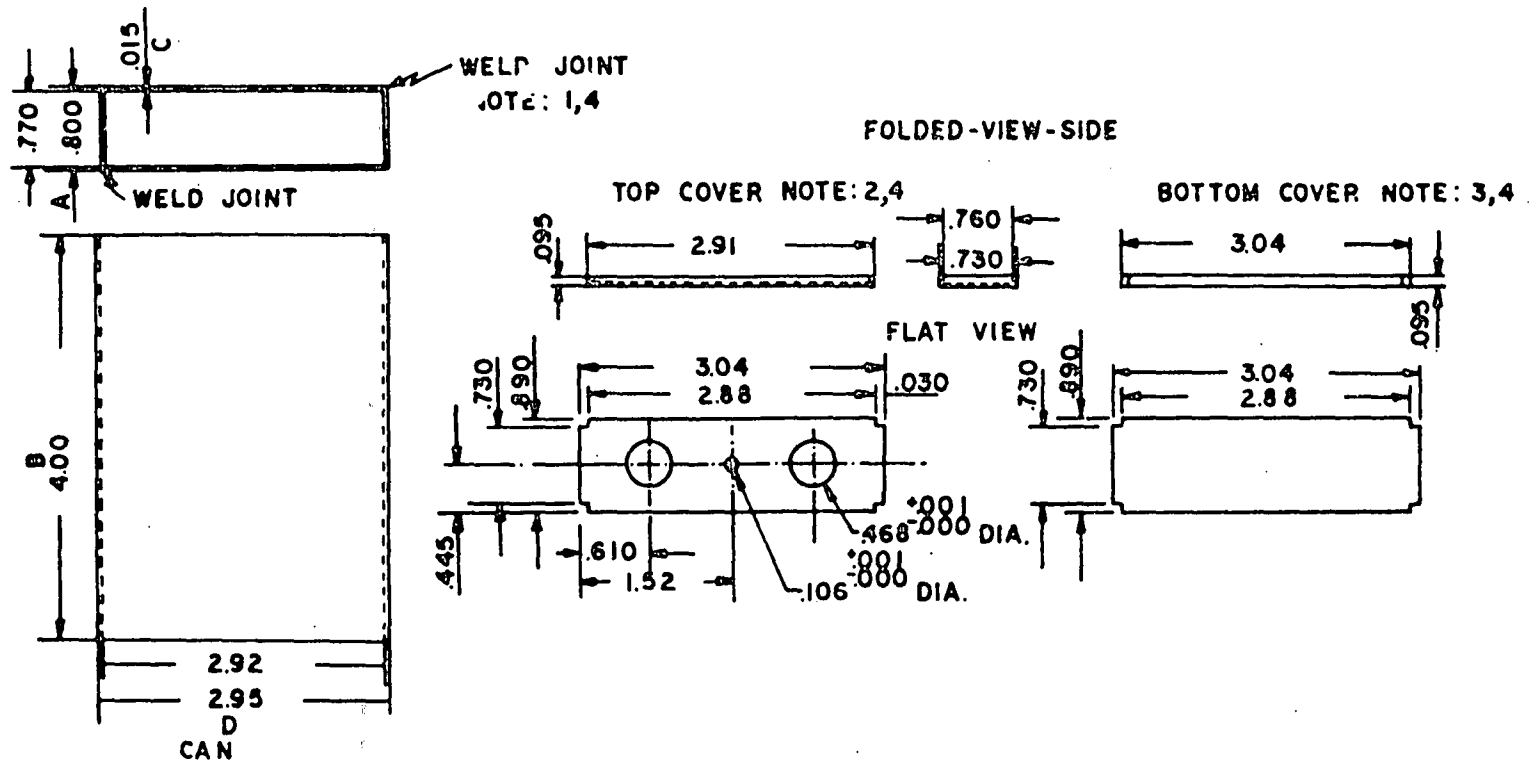   3 place ± 0.005   Inspected by:

Fig. I-8. Can assembly material 304L SS, Part No. T-12100

Attribute Sheet

Date:

Part No.:   T-12200
Part Name: Plaque Assembly
Vendor:
Lot No.:
Lot Size: Sample Size:

Dimensions	Pieces O.K.	Pieces not within tolerance
A. 0.300		
B. 0.300		
C. 2.80		
D. 3.25		

Tolerances:
   2 place 0.01
   3 place 0.005   Inspected by:
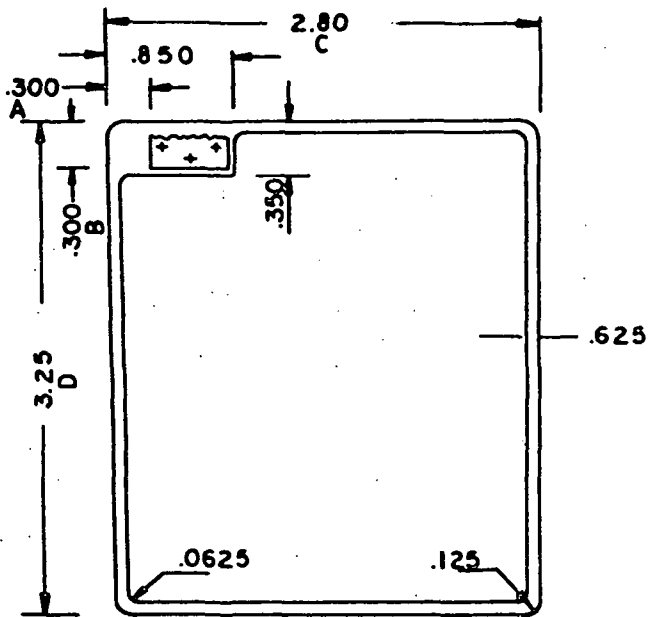
Fig. I-9. Plaque assembly, Part No. T-12200

Attribute Sheet

Date:

Part No.:   T-12019
Part Name: Nylon - Washer
Vendor:
Lot No.:
Lot Size: Sample Size:

Dimensions	Pieces O.K.	Pieces not within tolerance
A. 0.50		
B. 0.250 + 0.005 - 0.000		
C. 0.045		

Tolerances:
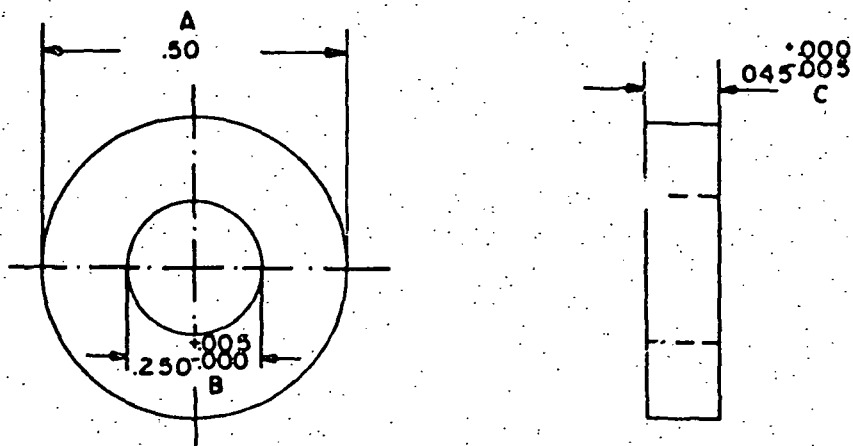   2 place ± 0.01
    3 place ± 0.005   Inspected by:

Fig. I-10. Washer material 6-6 Nylon, Part No. T-12019